Nuclear Engineering and Design 420 (2024) 113012

Contents lists available at ScienceDirect

Nuclear Engineering and Design

journal homepage: www.elsevier.com/locate/nucengdes

Improved Analysis of the Short-Term Station Blackout Accidents of the Peach Bottom Unit-2 Reactor with ASTEC Including Radiological Impact and Statistical Analysis with JRODOS

Onur Murat [a,*], Victor Sanchez-Espinoza [a], Fabrizio Gabrielli [a], Shisheng Wang [a], Robert Stieglitz [a], Cesar Queral [b]

[a] Karlsruhe Institute of Technology, Institute for Neutron Physics and Reactor Technology.Hermann-von-Helmholtz-Platz 1, D-76344 Eggenstein-Leopoldshafen, Germany
[b] Universidad Politécnica de Madrid, Alenza 4, Madrid 28003, Spain

ARTICLE INFO

Dedicated to the memory of Prof. Dr.-Ing. Robert Stieglitz, who passed away during the article revision process.

ABSTRACT

After the severe accident at Fukushima, the importance of BWR design and related structures and their contribution to the severe accident progression has increased. Fuel channel boxes, absorber crosses, water rods, and smaller primary containment design of the BWR have been considered in the ASTEC code to increase the knowledge of BWR design and associated models. The previously developed ASTEC model for Peach Bottom Unit-2 was updated to include modern GE14 10x10 fuel assemblies with realistic fission product inventories. The CASMO5 code predicted the fission product inventory and burnup for GE14 10x10 fuel assemblies based on real plant data obtained from the ENRESA samples. First, a Short-Term Station Blackout (ST-SBO) analysis was performed to compare the impact of the old and new fuel assembly designs on the accident progression and radiological consequences. Second, a short-term station blackout with a stuck open safety relief valve (ST-SBO SOSRV) was considered for modern fuel assemblies. The actuation of the safety valve resulted in a much lower corium ejection and a longer transient to basemat failure in the cavity. The scatter of corium ejection amounts between the considered scenarios showed the importance of the design of the bottom head and the penetration points in BWRs. In both cases, failure of the drywell head flange and release of radionuclides to the environment occurred. Higher burnup and radionuclide inventory in the 10x10 assemblies resulted in a larger release compared to the previous design. Radiological analysis using JRODOS was performed for both cases and the maximum total effective gamma dose rate was estimated to be 67.89 mSv/h and 119.46 mSv/h for ST-SBO and ST-SBO SOSRV, respectively. The statistical analysis and the number of records in the considered cities around the Peach Bottom Plant showed the distribution over the region and the risk factors of the populated cities. The collaborative use of three codes in this study allows users to identify the fission product inventory with CASMO5 and investigation of the severe accident scenario with ASTEC and identifying radiological impact of the released radioactive isotopes to the environment with JRODOS code.

1. Introduction

Severe accidents with large radionuclide release and dispersion over the environment and the public like Chernobyl and Fukushima have demonstrated the importance of analyzing and understanding of the severe accidents. In order to protect society and the environment, and to be able to take appropriate countermeasures in case of severe accident, the release of the radionuclides into the environment must be correctly predicted. To achieve this, the response of the power plant in the event of a severe accident must be modeled and evaluated using realistic fission product inventory to properly assess their radiological impact. Since the potential release of fission products after a severe accident depends strongly of the plant design and severe accident sequences, it is important to understand the nature of severe accidents and their radiological impact of different NPP design and operation using different codes such as ASTEC (Chatelard et al., 2016), MELCOR (Humphries et al., 2017), MAAP (EPRI, 2010), AC^2 (Wielenberg,et al., 2019), SOCRAT (Leonid,et al., 2019). The implementation of the BWR

* Corresponding author.
E-mail address: onur.murat@partner.kit.edu (O. Murat).

https://doi.org/10.1016/j.nucengdes.2024.113012
Received 10 August 2023; Received in revised form 2 February 2024; Accepted 9 February 2024
Available online 17 February 2024

specific structures (Chatelard et al., 2017), e.g. fuel channel boxes paved the way for the analysis of severe accidents of BWRs with the ASTEC code.

Approach of the previous study (Murat,et al., 2023), which involved implementation of the codes in order to examine the severe accident progression starting from estimating fission product inventory up to radiological release and impact to the public and environment, is also followed in this article. Fission product inventory and burn-up calculation in the previous study (Murat,et al., 2023) considered the 7x7 old type fuel assemblies and operation time was not publicly available and duration was assumed. Modern fuel assemblies designed for longer operational cycles of BWRs, to achieve higher burnup levels. However, higher burnup also means higher accumulation of fission products compared to old core designs. Since accident progression and loss of material integrity are due to the inability to remove the excess heat, higher burnup increases the potential damage in the event of beyond design basis accident. For this reason, consideration of modern fuel assemblies in severe accident analysis is needed for a better estimation of the accident progression as well as of the radiological consequences in addition to the improved understanding of the effectiveness of the safety system. The current GE14 10x10 fuel assemblies of BWR plants were modeled using the CASMO5 code (Rhodes,Ferrer and Hykes, 2022), and realistic burnup and fission product inventory were calculated based on available plant information, used to develop a new ASTEC model of the Peach Bottom Unit-2 ASTEC model. In addition, the new fuel assemblies contain Zircaloy water rods to increase the neutron moderation along the full core height. Hence, the oxidation of such additional structures will increase the release of energy and hydrogen generation in the core. Not only burnup, but also dimensional changes in the fuel assembly lead to changes in the amount of material and a higher proportion of zircaloy material, which drives the oxidation reaction and the accident progression during severe accidents.

In addition to the consideration of new fuel assembly design, the recirculation line was modelled in ASTEC in a more realistic manner using ASTEC components, e.g. volumes, pipes, junctions and connections, compared to the previous model (Murat,et al., 2023). It is worth to emphasize, as it was mentioned in the previous work (Murat,et al., 2023), that the design of the BWR includes specific components and the design of the containment. For a better prediction of the severe accident progression in BWR, it is necessary to consider all phenomena starting with the fission product inventory, release and transport from the core to containment and environment, and finally to predict the radiological dispersion.

This investigation represents one step ahead in the efforts to perform BWR severe accident analysis with ASTEC. The collaboration between KIT and IRSN allows the use of the source code and the implementation of BWR-related models and structures, which increases the range of applications of severe accident studies with ASTEC.

The Chapter 2 describes the extended ASTEC model of the Peach Bottom Unit-2. Following Chapter 3 presents the burnup analysis of the new fuel assembly design including assumptions for the calculation. Analysis of the Short-Term Station Blackout (ST-SBO) and the Short-Term Station Blackout with Stuck Open Safety Relief Valve (ST-SBO SOSRV) is presented in Chapter 4 and Chapter 5, respectively. Each transient analysis concludes with JRODOS radiological dispersion analysis.

2. ASTEC Model of Peach Bottom Unit-2 Nuclear Power Plant

A detailed description of the plant model, including vessel dimensions, volumes, connections, containment vessel, cavity, and defined physical phenomena, can be found in the previous study (Murat, et al., 2023). The differences in the core between the old and new designs are only in the design of the fuel assembly and the power level of the plant. Outside the vessel, the definition of the recirculation line has also been modified and implemented. Other than the updates and differences mentioned in this section, the rest of the design of the vessel and containment is the same as in the previous study and the details are described there.

Number of assemblies in the core is 764 and their distribution on each radial mesh 4, 60, 240 and 460, respectively, from inner most radial mesh to the outer most. The new fuel assembly design is GE14 10x10 and includes 2 water rods covering the space of 8 fuel rods in total. The dimensions of the new fuel assemblies are given in the next section which includes fuel inventory calculation. In addition, part length rods also exist in the assembly, however the NT-HEAT structure deals with decay and power profiles of fuel assemblies as one for this reason the definition of all rods considered as full length.

The definition of the new subchannel within the fuel assemblies is another step toward understanding the behavior of the new design fuel assemblies under severe accident conditions. Based on the neutronic calculations, water rods are placed in the BWR fuel assemblies to increase neutron moderation by providing liquid water at higher levels in the core. Additional around 8 % more Zircaloy material and coolant availability in the active region have a direct impact on accident progression, so the investigation of the new type of BWR fuel assemblies is necessary.

The previous design had two separate sections between shroud and vessel in order to provide a section for the recirculation line before the water is injected into the lower plenum. Because of this design, all core flow circulated in the recirculation line. The new design of the recirculation line provided separate sections for the driven flow and the suction flow domain and only one radial mesh which is called the “downcomer” constructed (Fig. 2–1).

The Description of plant design in recirculation line is updated to represent jet pumps and circulated flow (Fig. 2–2). The water inlet from the “DCTOP” volume is connected to the “downcomer” channel and then flows through the recirculation lines named “JET_L11″, ”JET_L12″, “JET_L13″ for the first train; ”JET_L21″, “JET_L22″, ”JET_L23″ for the second one. Then, the combination of these two flows enters the “NOZZLE” pipe structure, which has a decreasing flow area on the downstream. The suction flow from the downcomer represented by the volume “DCTOP”, the junction “DCTMIX1″ and the volume ”MIX_1″. The junction “MIX2MIXDF” connecting the volume “MIX_1″ and the pipe structure ”MIXDIF“ provides intake flow to be injected into the lower plenum along with the flow driven by the jet pumps.

The containment and reactor building zone definitions and primary containment failure modes have not changed (Fig. 2–3). To recall the failure modes: The first describes a rupture between the wetwell zone and the torus space when the pressure in the wetwell zone exceeds 1.2 MPa. The second mode describes a rupture between the drywell and the refueling bay when the temperature reaches 644 K and the pressure exceeds 0.565 MPa. Pressure dependent break increases from 0.0 m^2 (at 0.565 MPa) up to 0.04 m^2 (at 1.378 MPa). This harsh environment attacks the flanges in the head of the drywell. Representation of the primary containment vessel of the reactor and building sections with their connections between them are presented in Fig. 2–3. First failure mode described with valve-400 (in red) and connection F400 (in red) between wetwell (WW) and torus room (RB-TORUS), second failure mode defined with valve-398 (in red) and connection F398 (in red) between drywell (DW) and refueling bay (RB-REFUE).

In terms of considered physical phenomena, in addition to the previous design, the described water rods were included in the RADASSEM module for calculating the radiative heat transfer calculation in the area

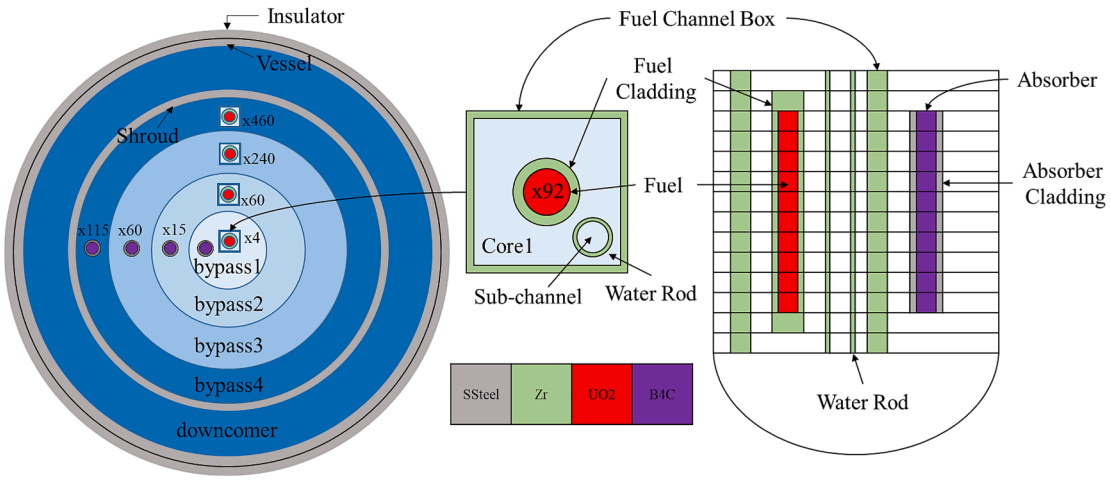

Fig. 2–1. ICARE radial meshes (left) and axial meshes (right) of the updated core design with fuel channel box (BOX4SIDE) and absorber structure equivalents in the each channel.

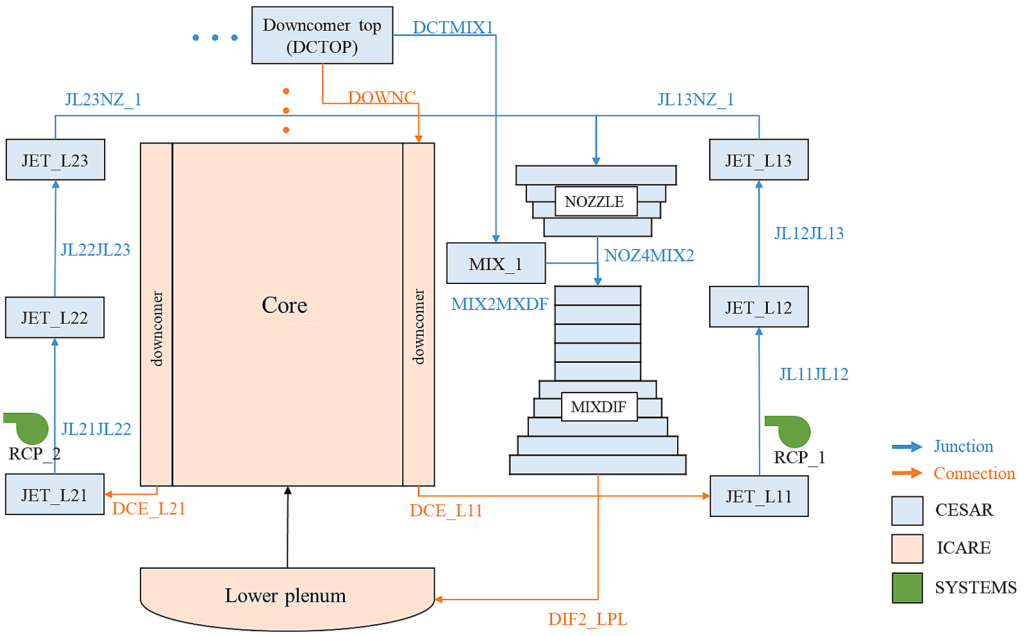

Fig. 2–2. Recirculation line CESAR volumes, junctions, ICARE core domain and their connections of RPV of Peach Bottom Unit-2 ASTEC Model.

of the fuel channel boxes, since the water rods are located between the fuel rods. The water rods are made of Zircaloy and their oxidation kinetics are defined by the ZROX module with the best-fit option enabled. Since the water rods are also in the active region, the definition of their mechanical behavior and the relocation of the molten material is important for the accident progression. For the water rods, integrity criteria was set to the 2500 K which is also defined for the Zircaloy fuel channel boxes. Structure condition was changed to the DISLOCAT when the temperature of the water rod reaches the limit value.

The boundary conditions of the plant are also updated to catch up with the new stationary conditions of the plant. The connections of the water injections, called "FWATER", are described. The number of feedwater lines is 4 and each injection is 523.17 kg/s at 468.65 K. The boundary conditions at the steam line were defined as pressure boundary conditions and 7.2285 MPa was set to correspond to the design pressure of the upper plenum of the pressure vessel. The rest of the boundary conditions already defined in the previous study were kept unchanged.

3. Fuel Inventory Calculation with CASMO5

Decay heat level of the fuel assemblies is the key element in order to simulate accident progression from the fuel integrity lost up to environmental release and evaluation of the public safety. Depending on the burnup level of the fuel and corresponding fission product inventory decay heat level and the accident progression and timing of the important points in-vessel and ex-vessel domain can change.

The first authorized power level of the Peach Bottom Unit-2 power plant was 3923 MWth and the initial fuel load consisted of 7x7 fuel assembly types which is used in the previous study (Murat,et al., 2023). In the following years, the power was increased; initially 3458 MWth in 1994, 3951 MWth in 2014, and finally 4016 MWth in 2017 (Exelon Generation Company, 2018). U.S. storage databank of the discharged fuels from the operational power plants between 1968 and 2013 (Hu, et al., 2016) showed that 10x10 fuel design selection became the only design layout for the BWRs after 2010 s. In addition, a previous study using MELCOR for the Peach Bottom NPP analysis in 2013 considered the GE14 10x10 BWR fuel assembly design (Bixler et al., 2013).

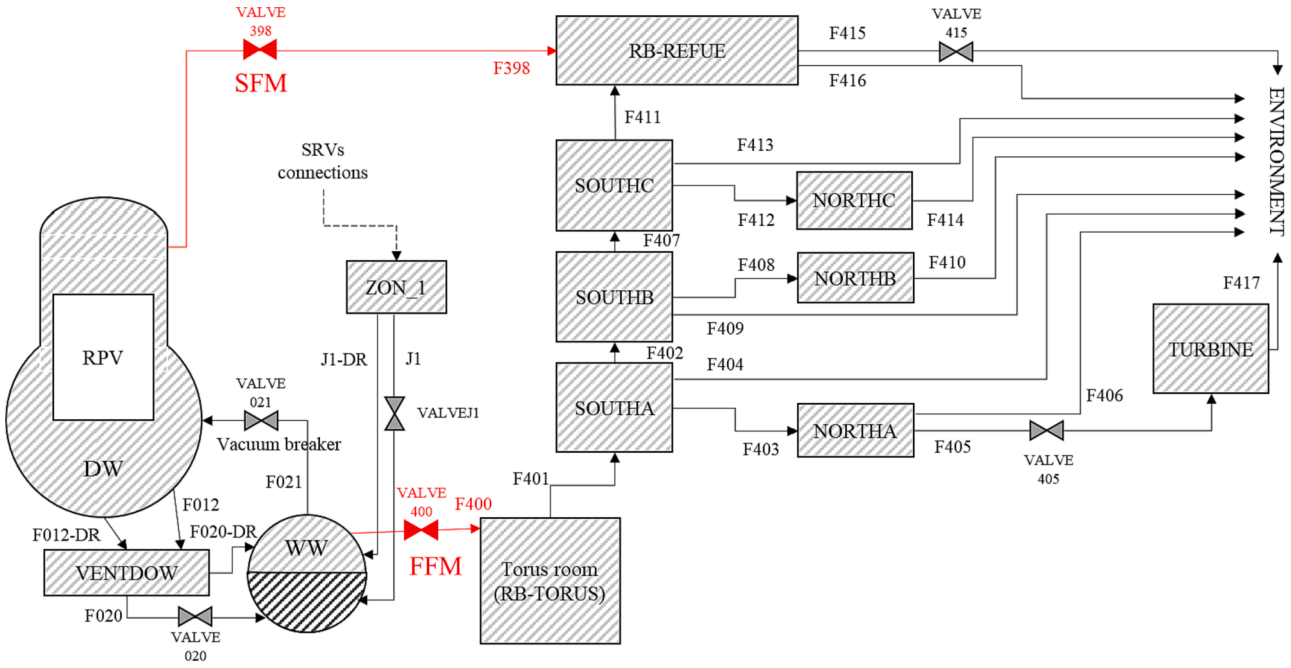

Fig. 2–3. Primary containment vessel and reactor building modelling of Peach Bottom Unit-2 ASTEC model in CPA module.

Although the study was conducted prior to the recent power upgrade, it was assumed that the same fuel assembly design and type would continue to be used in the reactor core. The product portfolio of General Electric, the fuel supplier, has the same type of fuel assemblies as today, which also supports this assumption.

The two-dimensional neutron transport code CASMO5 was selected for the burnup calculation of the GE14 10x10 fuel assembly. The code is capable of modeling geometries at the pin or fuel assembly level, including burnable absorbers, fuel assembly support structures, water channels, or placement of antisymmetric structures. Burnup calculations also consider thermal expansions and densities for each pin cell (Rhodes, Ferrer and Hykes, 2022). In order to build a model of the fuel assembly, dimensions of the structures are given in Table 3–1, and the material composition and placement of the rods are given in Table 3–2. Diagonal crossed sections in the Table 3–2 represents the water rods which each occupying a space of 4 fuel rods.

Experimental program which deals with an extracted fuel rod from the Forsmark 3 NPP in Sweden was followed. The GE14 10x10 type fuel assembly was used between July 2000 (cycle 16) and 28 May 2005 (cycle 20) in the plant and isotopic concentration analysis was carried out (Gauld and Mertyurek, 2018). The operation of the fuel assembly in the core lasted 1792 calendar days, including 5 burning cycles. Neutron criticality analysis study for the fuel assembly (Martinez,et al., 2015) showed that cycle lengths were approximately 354 days, 270 days, 320 days, 487 days and 293 days. The remaining days were considered

Table 3-1
GE14 10x10 fuel assembly dimensions (Rochman,et al., 2022), * (Radaideh et al., 2019).

Parameter	Value (cm)
Fuel radius	0.438
Cladding inside radius	0.447
Cladding outside radius	0.513
Fuel rod pitch	1.295
Active fuel length	368.0
Part length rod length	220.8
*Water rod inside diameter	2.321
*Water rod outside diameter	2.521
*Fuel channel box inside length	13.406
*Fuel channel box outside length	13.914

Table 3-2
GE14 10x10 fuel assembly rod placements and enrichments (Lawing,Palmtag and Kropaczek, 2021).

Fuel Type	U-235 w/o	Gd w/o
1	1.6	0.0
2	2.8	0.0
3	3.2	0.0
4	3.6	0.0
5	3.95	0.0
6	4.4	0.0
7	4.9	0.0
5G	3.95	8.0
6H	4.4	6.0
7G	4.9	8.0
7H	4.9	6.0

refueling periods and 17 days were evenly distributed between burning periods as an assumption in this study. Within the scope of the analysis of ENRESA samples in the GE14 10x10 assembly rod, moderator density at the axial elevation 1.91 m was stored for each burning cycle (Martinez,et al., 2015). The cycle average moderator densities are 0.317 g/cm^3, 0.374 g/cm^3, 0.324 g/cm^3, 0.540 g/cm^3 and 0.584 g/cm^3 for cycle 1 to 5, respectively.

In addition, information on fuel and moderator temperature, void fraction, and specific power is required for CASMO5 burnup analysis. The fuel temperature (792 K) and moderator temperature (560 K) were selected from the previous study on ENRESA samples (Rochman,et al., 2022). Exit void fraction of the assemblies in the BWR can vary up to 80 % depends on the position of the assembly in the core. The previous study of the axial moderator density distribution and burnup for GE14 10x10 fuel assemblies showed that void fraction distribution for each assembly across the core (Marshall et al., 2016). Distribution of the void fractions are given in top left image in Fig. 3–1. The blue line represents the minimum and the red line the maximum of the achieved void

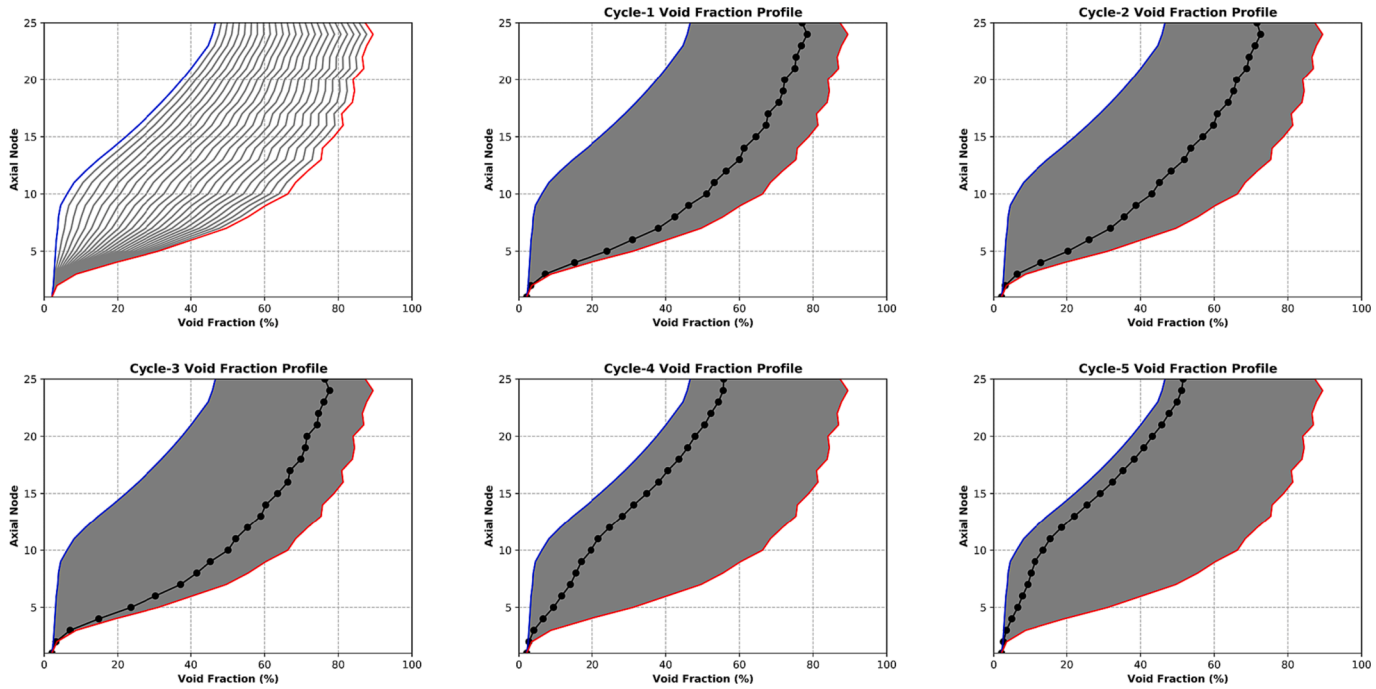

Fig. 3–1. GE14 void fraction profile sampling (Marshall, Ade and Bowman 2016) and selected void fraction profiles for each cycle.

fraction profiles. Since the power level and heat are not generated uniformly radially in the core, the void fraction along the fuel assembly depends on its specific position in the core for each burning cycle. Information on fuel assembly positions in burning cycles is operational data and not publicly available. The known information about the void fractions of the fuel assemblies is that they must lie between the maximum (red) and minimum (blue) void fraction profiles. The number of fuel assemblies in the core is 764 and based on this information, 764 void fraction profile samples between the maximum and minimum profiles were created. At each axial node, the difference between the maximum and minimum void fraction profiles is divided into 764 and the production of the samples is based on this approach to obtain the pattern information between the known maximum and minimum profiles.

The moderator density at the axial height of 1.91 m (13th node) provided information about the selection of the void fraction profile for

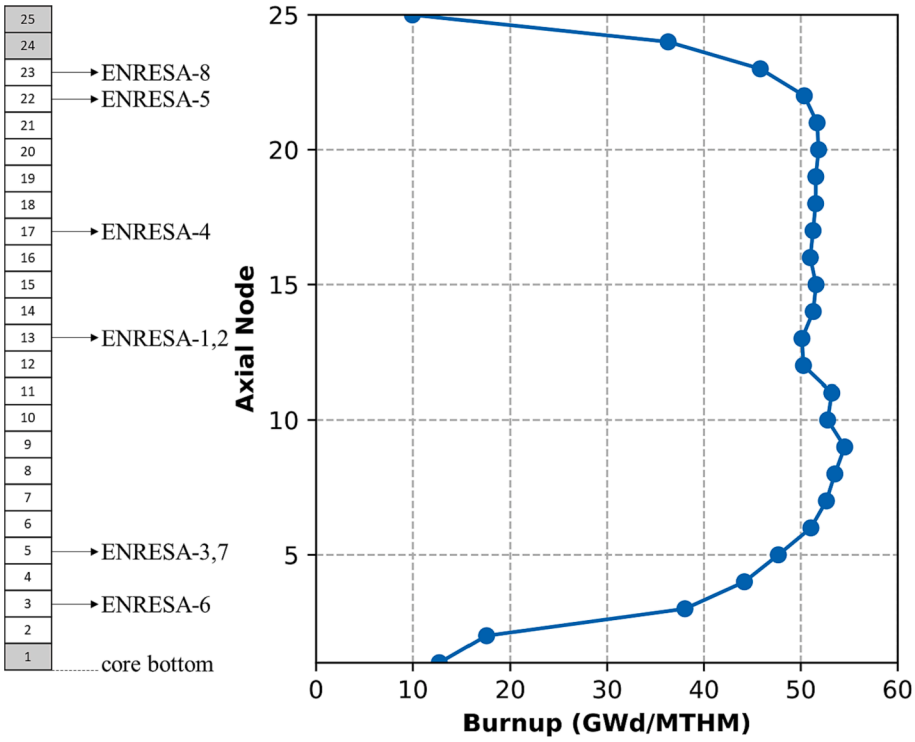

Fig. 3–2. Selected fuel rod sections from GE14 10x10 fuel assembly (Gauld and Mertyurek, 2018) and axial burnup profile of the rod (Marshall, Ade and Bowman 2016).

each cycle. The average moderator density can be calculated using the phase densities and void fraction of the moderator. An operating pressure of 7 MPa was used to calculate the phase densities, and all values of the 13th node were searched among the 764 void fraction profiles generated to determine the average moderator density. The matched void fraction profiles are indicated with dotted lines for each cycle in Fig. 3–1.

Based on the U.S. stored fuel database (Hu,et al., 2016), the average specific power of BWR fuel assemblies is 24 MW /MTU. However, a previous study considering the criticality calculation during the transport of the GE14 10x10 BWR spent fuel in a cask assumes the specific power of the fuel to be 25 MW /MTU (Radaideh and Price, 2018). Since the repository database also contains the old fuel assembly types, the specific power for the CASMO5 calculation was chosen to be 25 MW /MTU. The distribution of power along the fuel rod was based on the burnup profile of the GE14 10x10 fuel assembly from the previous study (Marshall et al., 2016). The burnup profile is related to the average neutron flux in the corresponding sections, which also contains information about the specific power. The profile shown in Fig. 3–2 was used and the specific power was assigned to each of the 25 nodes of the fuel assembly section. The power values were adjusted so that the average specific power was 25 MW/MTU.

Dimensional and material data constructed the assembly for the CASMO5 input deck. Fuel rod temperature, moderator, void fraction, specific power, and burn time were used to perform burnup simulations for 25 axial nodes of the GE14 10x10 assembly. Discharge burn up of 46.47 MWd/t was calculated for an assembly and same burnup level was assumed for all 764 fuel assemblies in the core. Although the fuel assembly burn up levels are not the same throughout the core, the consideration of a high burn up level for each assembly played a role in the worst-case scenario of high fission product levels for the accident scenario and fission product dispersion. The calculated fission products feed the decay heat module ASTEC ISODOP and the fission product inventory for severe accident analysis.

4. Analysis of the ST-SBO for Peach Bottom Unit-2

The following ASTEC calculation modules have been activated to perform the analysis: CESAR, ICARE, CPA, ISODOP, SOPHAEROS, RCSMESH, MEDICIS, RUPUICUV, CORIUM and DOSE for plant analysis. A steady state analysis was performed and then the ST-SBO accident scenario was created. The same accident transient from the previous study (Murat,et al., 2023) was used to compare the old and new fuel design in terms of accident progression and source term study. ASTEC version V2.2 Revision 6790 M developer version was used as in the previous study.

4.1. Stationary Plant Conditions at Nominal Power

After the plant changed the fuel assembly type and power upgrade approved (Exelon Generation Company, 2018), updated safety analysis report (U.S. Nuclear Regulatory Commission, Peach Bottom Atomic Power Station, Units 2 and 3, Revision 27 to Updated Final Safety Analysis Report, Chapter 1.0 2019) was prepared based on the new plant parameters.

A comparison of updated design parameters in Figure 1.6.2 in the updated safety analysis report (UFSAR) and the ASTEC model results is given in Table 4–1. Stationary results were obtained for 500 s. The total mass flow in the updated core design were kept at the same value as in the earlier report, which included the core design and operating data (Larsen, 1978). Therefore, the core flow, bypass flow, and recirculation flow rate taken from that study. The updated modeling of the recirculation line in the ASTEC input deck allows a comparison between the design parameters of the jet pump and the ASTEC model. The jet pump efficiency is defined by multiplying the N and M ratios, the definitions were made in the analysis study for the BWR jet pump loop

Table 4-1
Updated design parameters and stationary results of Peach Bottom Unit-2 ASTEC model.

Design Parameters from UFSAR		ASTEC
Core Power (MWth)	4016	4016
Feedwater mass flow rate (kg/s)	2092.69	2066.58
Total mass flow rate (kg/s)	12914.78	12924.62
Core mass flow rate (kg/s)	11336.75	11330.04
Bypass mass flow rate (kg/s)	1578.03	1577.20
Recirculation flow rate (kg/s)	4309.12	4309.10
Jet Pump N ratio	0.16	0.16
Jet Pump M ratio	1.96	1.99
Feedwater temperature (K)	468.65	468.65
Dome pressure (MPa)	7.239	7.239
Driven flow temperature (K)	548.98	547.03

(Narabayashi,et al., 2006).

M Ratio definition by the ratio of suction flow rate and driving flow rate. The source of the suction flow is the water inlet in the downcomer and is driven by the driving flow rate which is travel through recirculation line. After that the injected flow from the nozzle drives the suction stream into the normal throat and flow area increases while the mixed stream flows downward. At the exit of throat section water flows into the lower plenum. The ratio of the pressure differences, i.e. the pressure rise from the suction region to the exit and the pressure drop from the injection nozzle to the exit defines the N ratio.

4.2. Short Term Station Black-Out Accident

Previous publication and selection of the transient ST-SBO was based on the highest core damage frequency at BWR plants (U.S. Nuclear Regulatory Commission, Severe Accident Risks: An Assessment for Five U.S. Nuclear Power Plants, NUREG-1150 1990). In order to make a comparison between the old 7x7 fuel assembly design and the new GE14 10x10 fuel assembly, the same transient scenario from the previous study was chosen (Murat,et al., 2023). Not only the design, but also the difference on the power level is significant factor when studying the accident progression. The basis for selecting the scenario was the safety analysis study (Kolaczkowski,et al., 1989) for Peach Bottom Unit-2 and the highest core damage frequency belongs to the station blackout accident.

The accident scenario begins with the loss of offsite power, the failure of all AC and DC power at the plant except the DC power to start and control safety relief valves and ADS without considering any ECCS system (HPCI, RCIC, etc.). The steam extraction and feedwater injection lines are then closed to isolate the core from the outside world. Then SRV-1 operates for 200 s until the operator takes control of a manual action of a safety relief valve. The operating range of the safety valve was set to 6.49 MPa to 7.18 MPa and the procedure continued until the water level in the core reached one-third of the core. Then the automatic pressure relief system (ADS) was activated and SRV-1, SRV-2, SRV-3, SRV-5, and SRV-6 were opened to relieve the pressure in the vessel. The simulation continued until the rupture of the basemat which responsible for holding the molten material ejected from the vessel into the containment.

4.2.1. Main results of ST-SBO transient

The sequence of events from the previous study (Murat,et al., 2023) and the new fuel assembly design with upgraded power level was compared and the results are given in Table 4–2. The order of events is given chronologically.

The power history and burnup level are the main parameters that determine the excess heat after the reactor is shut down. To understand the differences between the core loaded with 7x7 fuel assemblies and the new upgraded core loaded with 10x10 fuel assemblies in terms of excess heat, the power levels of the cores for 1 h after the scram are shown in

Table 4-2
Comparison of the sequence of events between new and old design fuel assemblies in Peach Bottom Unit-2 ASTEC Model ST-SBO scenarios.

Sequence of Events	Time (s) (10x10) ST-SBO	Time (s) (7x7) ST-SBO (Murat, et al., 2023)
SRV-1 starts operation	0	0
SRV-1 stops operation, Manual operation of a SRV starts	200	200
First cladding creep rupture, start of the fission product release	524	1037
First material slump in lower plenum	622	1142
First slump of corium with fission products in lower plenum	643	1158
First appearance of a cavity in core	648	1167
Manual operation of a SRV stops, ADS actuates	4782	3867
First total core uncovery	9959	6772
Lower head vessel failure	21,616	13,361
PCV head flange failure	26,137	13,415
Basemat rupture	100,576	88,142

Fig. 4–1. The residual power of the cores drops rapidly and after that the decay heat, corresponding to the fission product inventory, takes responsibility for the excess heat production in the core. During the power decay, the general trend shows that the difference between the old and the new assembly is about 10 MW at the end of the first hour.

Higher power associated with higher temperatures in the core and earlier loss of integration of materials. Fuel cladding rupture and release of fission products occurs after 524 s in the new type of fuel assemblies, which is almost half the duration of the previous calculation with the old fuel type. The first material slump in the lower plenum and the appearance of the first cavity in the core also occur more quickly with the new fuel assemblies. On the other hand, this fast transient trend does not appear when stopping the manual operation of the SRV and the ADS actuation. This situation can also be seen in Fig. 4–2, which shows the vessel pressures and depressurization actions with ADS operation. The system pressure held almost 1000 s longer in the core loaded with new assemblies compare to old type fuels.

The ADS is put into operation when the water level in the core reaches one third of its level. To understand the depressurization transient of the core, the water level must also be tracked. A comparison of the water levels between the old and new assembly types during the accident transient up to total uncover is shown in Fig. 4–3. The dashed blue line represents the water level of the DCTOP volume containing the water source for the lower plenum transfer, and the dashed blue line with the star mark represents the water level in the core. Red solid lines were used for the case of a new type of fuel loading and the marked line is again representative of the core domain.

The water level drops rapidly and reaches the top of the core after about 300 s for the 7x7 type fuel assembly loading. Thereafter, the water level continues to drop rapidly until the operation of ADS, and depressurization causes a sudden rise in the water level in the core. The change in water level for the core loaded with a new 10x10 fuel shows a gradual decrease. Start of the fission product release is seen 524 s which is earlier than the point which water level reaches top of the active fuel. The integrity condition of the cladding material is defined based on the temperature and oxide scale growth on the surface. If the temperature of the cladding reaches 2500 K or temperature reaches 2300 K with oxide thickness less than 250 μm cladding material allows to fission product transport. Since the high level of burned fuel assemblies are distributed over the entire core, high residual power and temperature build up triggered the temperature driven integrity condition of the cladding material and fission product release.

The updated modeling of the recirculation line allows for recirculation of one-third of the total core flow as it was intended in the plant. For this reason, when the reactor is shut down, only one-third of the total core flow is stopped and the remaining water supply in the downcomer feeds the core. The old recirculation line design in the previous publication (Murat,et al., 2023) deals with recirculation considering the total core flow. When the reactor is shut down, the operation of the recirculation pumps is stopped and the total core flow is reduced and the core suffers from water shortage very quickly. The updated new recirculation model allows to observe a more realistic behavior of water recirculation and water level in the core after shutdown. The depressurization of the core at 4782 s shows an increase in water level to the top of the core, which was not observed in the previous model. The reason for that, the time step for the previous calculation was 1.0 s during the ADS operation, while the updated transient core calculation has a time step of 0.5 s,

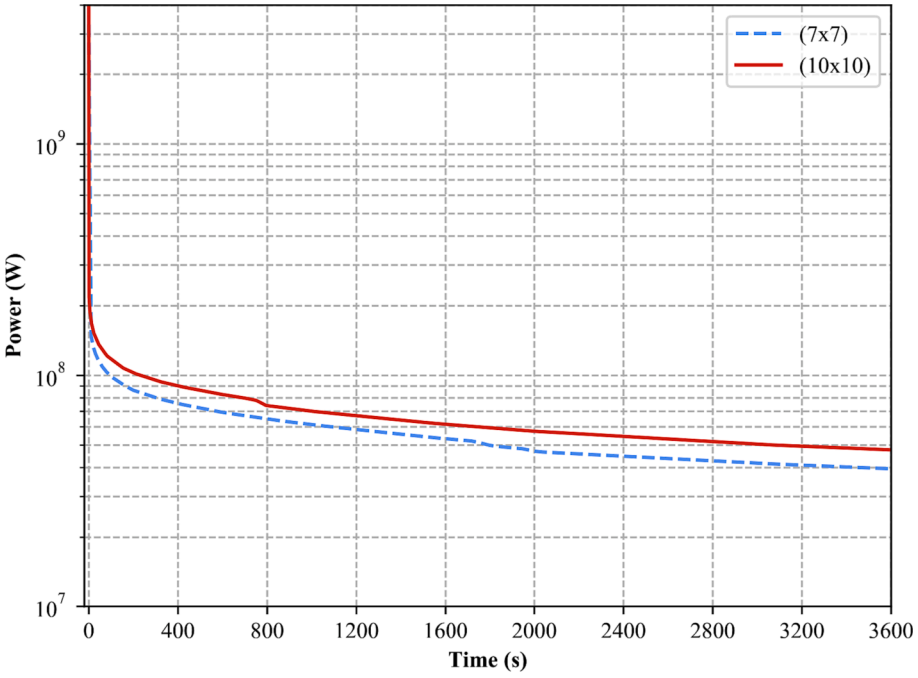

Fig. 4–1. Power comparison between the cores loaded with new and old design of fuel assemblies.

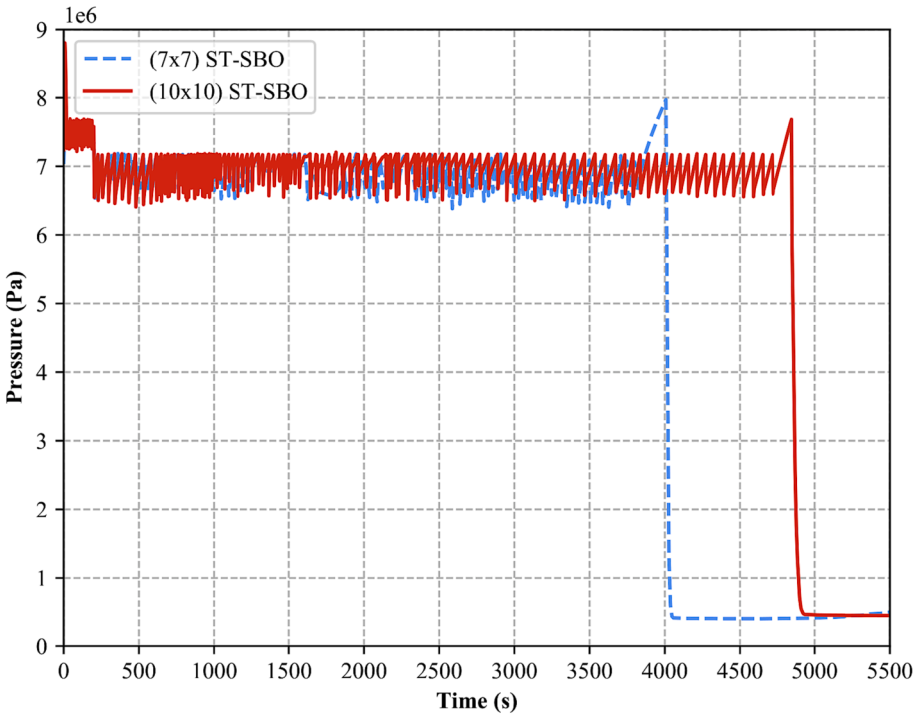

Fig. 4–2. Vessel pressure comparison between the cores loaded with new and old design fuel assemblies during automatic SRV-1 and manual SRV operation.

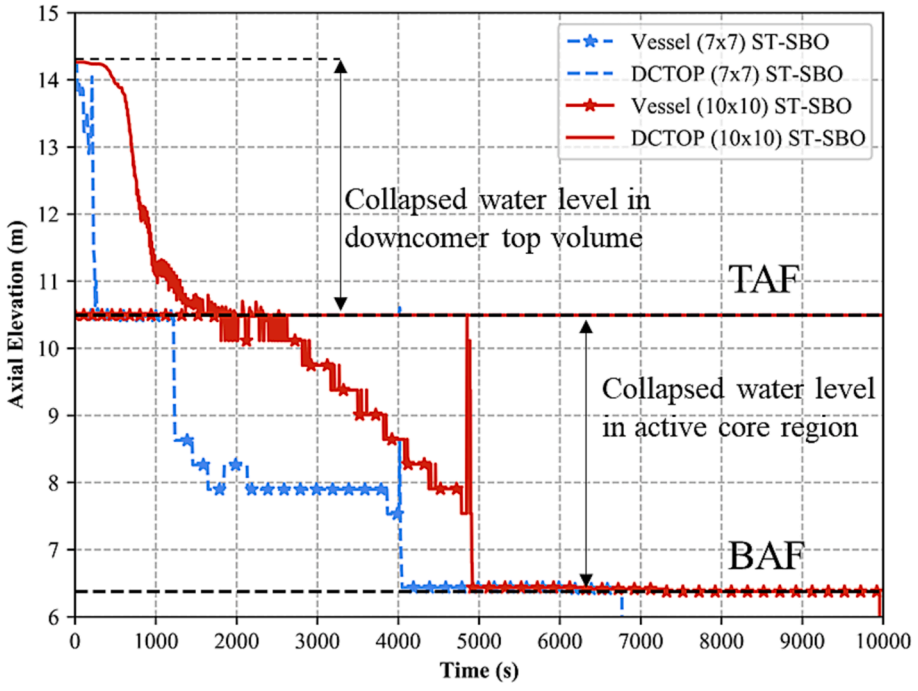

Fig. 4–3. Water level comparison inside the vessel (ICARE domain) and top of the downcomer (DCTOP) between the models loaded with new and old design fuel assemblies.

which is capable of capturing the entire rise in water level. For this reason, the ADS operation results a steam flash up to top of the core in both cases. The total uncover of the core event was stored at 9959 s, when the water level dropped below the core bottom level. The definition of the lower plenum in ASTEC includes only one mesh, so the database stores 0.0 below the axially lowest mesh in the core.

The rise of the water level during the accident determines the duration of the steam environment in the core. The steam environment and high temperatures drive the exothermic oxidation reaction that leads to hydrogen production and energy release, damaging the structures in the core. The total hydrogen mass produced in the vessel by oxidation for both cases is shown in Fig. 4–4. The core of the new 10x10 fuel assembly is shown with red solid lines and the old fuel assembly model is shown with blue dashed lines in the figure. In addition, the hydrogen masses produced by the different materials are shown with markers for both cases. Since the steam environment was in the active

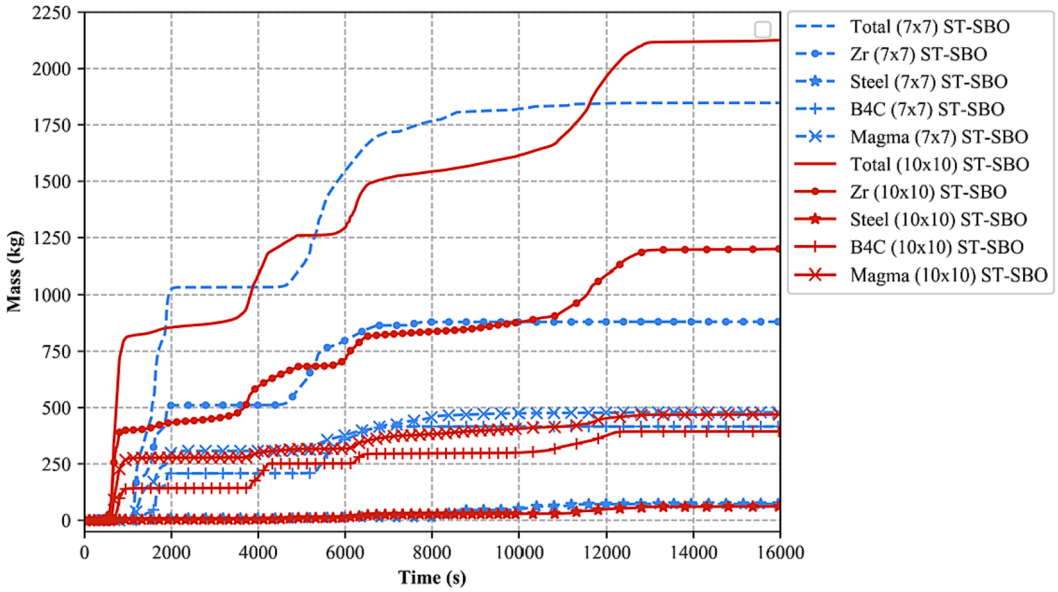

Fig. 4–4. Hydrogen mass comparison between the cores loaded with new and old design fuel assemblies.

core region longer for the core with new assemblies, a larger amount of hydrogen generation was observed. The oxidation reaction builds up more rapidly in the previous study with 7x7 assemblies because the water shortage begins earlier and a rapid increase is observed when the water level reaches at the bottom mesh points in the core. However, the new model was exposed to liquid water for a longer period of time and the water supply in the active core region does not allow the oxidation reaction to build up as quickly as the previous model. Immediately after the core is fully exposed by around 10,000 s, the oxidation of Zircaloy increases and so does the hydrogen production. The total hydrogen production in the vessel for the core loaded with 7x7 assemblies was 1847.6 kg and for the core loaded with 10x10 assemblies recorded 2138.3 kg.

Because the new fuel assembly is designed and sized differently than the previous fuel assembly, the amount of material that can potentially create a chemical reaction is also different in the core. The water rods contribute about 2800 kg of Zircaloy material to the core, and not only the water rods, but also the new 10x10 fuel assemblies contain about 2500 kg more Zircaloy than the 7x7 fuel assemblies due to the dimensions of the fuel channel boxes. The changed dimensions also play a role in the fuel element cladding, therefore about 500 kg less cladding material was used for the fuels placed in 10x10 assembly design.

Degraded materials move downward in the core and the resulting material accumulation in the lower plenum. Molten and mixed structures are referred to as magma in ASTEC terminology, and their stratification is shown in Fig. 4–5. Magma layers numbered 2 and 3, corresponding to the oxide layer and the light metal layer, accumulate and debris formation observed on top of them. The failure of the lower head was stored at 21,616 s and a total of 210.48 tons of corium were ejected from the vessel into the containment cavity. For comparison with the previous model, the amount of ejected material with the core loaded with old fuel elements was 152.34 tons. After the accumulation of magma in the lower plenum, the rupture point on the wall of the lower plenum determines the amount of ejected material. The axial position of the failure mesh was between 0.49 and 0.69 m from the bottom of the hemispherical part of the lower plenum in the previous

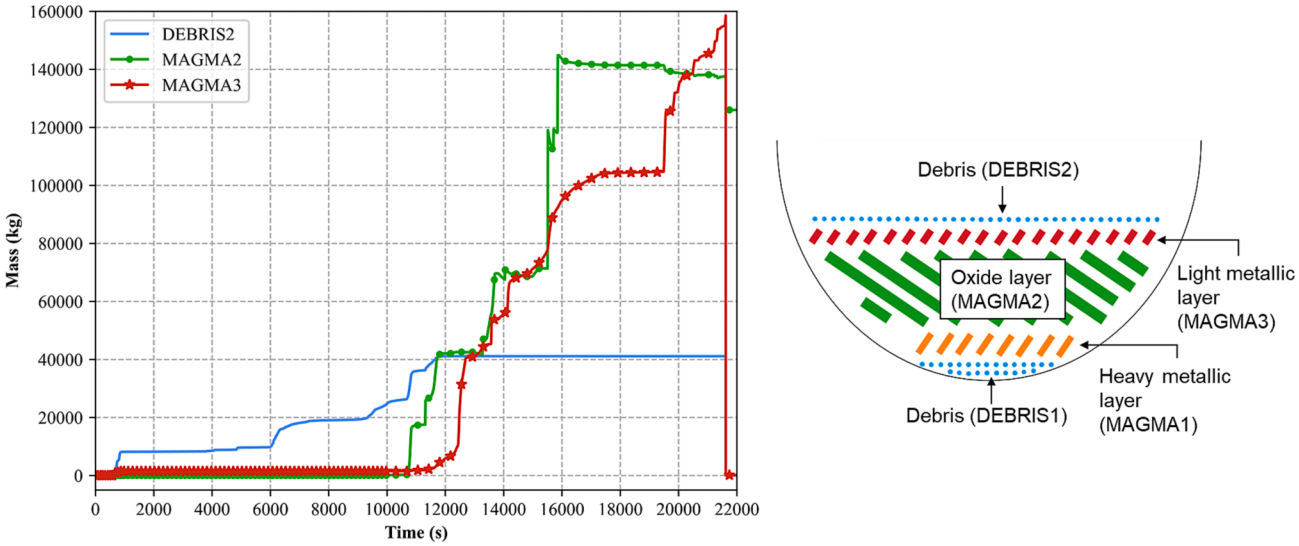

Fig. 4–5. Corium mass accumulation for 10x10 fuel assembly ST-SBO scenario up to failure in the lower plenum (left) and ASTEC typical debris configuration in the lower plenum (right).

study. The results for the new core show that the position of the failure mesh is between 1.39 and 1.65 m axially from the bottom of the vessel. Despite the fact that the failure point of the new model is axially higher, the amount of corium mass ejected from the lower plenum is higher. Early loss of material integrity and relocation in the lower plenum and a prolonged period of in-vessel scenario and lower head failure resulted in a higher amount of corium ejection despite the fact that the lower plenum wall failure was axially higher compare to previous study.

The corium ejected from the lower plenum was transferred into the cavity zone and the in-vessel phase of the accident ended. As the safety relief valves were actuated and the core depressurized, the temperature and pressure in the primary containment vessel increased. After the failure of the lower plenum, the transferred magma structures increased the temperature in the cavity and in the drywell. The pressure level in the drywell was already above the described limit for the second failure mode. At a temperature of 644 K and a pressure value of almost 900 kPa, a pressure-dependent rupture occurred between the drywell zone and the refueling bay zone at 26,137 s (Figs. 4–6). The rupture between the drywell and the refueling bay opens a pathway for the fission products into the environment. Since the definition of the break depends on the pressure difference between the drywell and the refueling bay, fluctuating pressure values around 600 kPa were recorded when opening and closing the connection.

The accident progression lasted longer in the ex-vessel phase for the new core and model compare to previous study. From the beginning of the accident, the water inventory in the vessel prolonged the phase inside the vessel and the failure of the lower plenum. The depressurization of the core by the ADS and the failure of the lower plenum resulted in significant pressure increases at 4782 s and 21,616 s.

Based on the calculation using the CASMO5 code to determine the fission product inventory and burnup level, the inventory of fission product masses is given in Table 4–3. The following columns represent the fractions of the inventories at the end of the calculation. The primary column corresponds to CESAR volumes describing the vessel and recirculation lines, the containment column corresponds to CPA zones defining the primary containment and the reactor building.

Storage of released fission products in the environment collected and used for the next step of the accident analysis, namely the investigation of the effects of the released substances on the public. For this purpose, the JRODOS tool was added to complete the study.

Table 4-3
Fission products mass inventory and their fractions in the considered domains at the end of the calculation for ST-SBO transient.

Elements	Inventory (kg)	Primary	Containment	Environment
Kr	68.60	0.105	0.499	0.264
Xe	1025.79	0.105	0.499	0.264
I	36.66	0.172	0.664	0.025
Sb	2.81	0.115	0.572	5.38E-4
Te	93.41	0.141	0.449	3.95E-4
Ag	7.30	0.206	0.657	5.53E-4
Cs	556.56	0.185	0.698	6.77E-4
Rh	79.54	9.85E-5	2.02E-4	1.66E-8
Mo	644.51	0.096	0.402	2.78E-4
Ba	290.09	0.230	0.323	8.08E-5
Sr	166.72	0.152	0.029	6.59E-6
Y	87.65	9.72E-5	1.98E-5	6.21E-8
Nb	3.80	0.0	0.0	0.0
Ru	479.17	0.088	0.160	1.98E-5
Ce	502.68	0.128	0.115	2.71E-5
La	236.88	0.067	0.031	7.09E-6
Eu	27.98	0.049	0.021	4.24E-6

4.3. Statistical Analysis of the Fission Products Dispersion and Worst-Case Scenario Approach for ST-SBO Investigation with JRODOS

Starting from the fission product calculation with CASMO5 code and following ASTEC severe accident analysis of the Peach Bottom Unit-2 Plant, JRODOS analysis was conducted to evaluate the public safety risk based on the released radioactive isotopes to the environment. The amount of the radioactive isotopes released to the environment from the containment vessel failure to the end of the simulation was collected and a total of 2.19E+18 Bq activity release recorded. Main radioactive fission products were selected to present in Table 4–4 based on their volatility and their radioactivity level which have potential treat for public safety (Sehgal, 2012). The cumulative amount of the some isotopes shows decrease up to end of the simulation since those isotopes have relatively short half-life, order of hours, compare to the others such

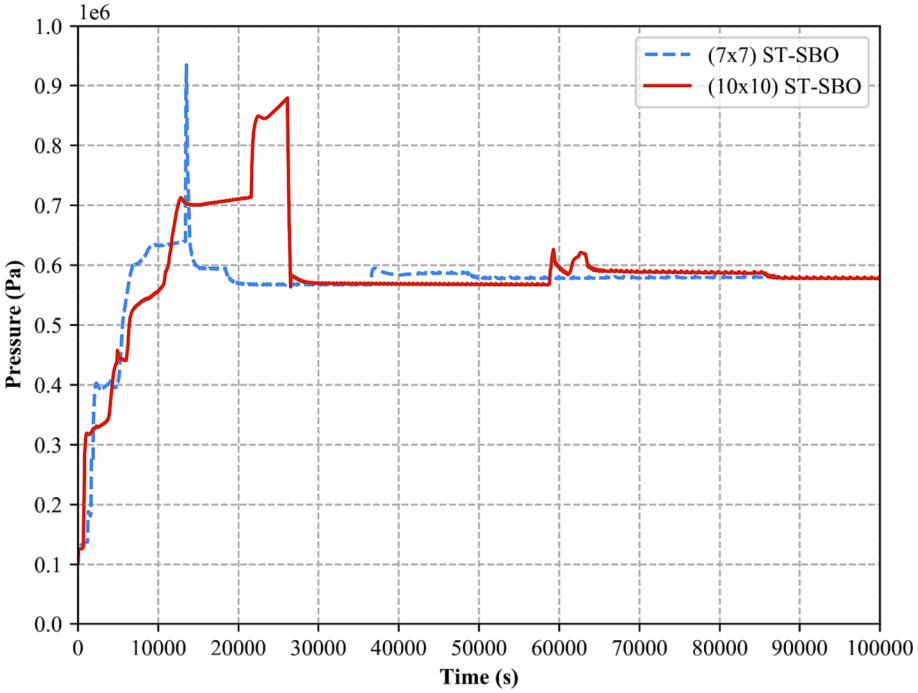

Fig. 4–6. Drywell Zone pressure comparison between the models loaded with new and old design fuel assemblies.

Table 4-4
Total mass of radioactive fission products released to the environment at the end of ST-SBO scenario.

Isotope	Half life	Release (kg)	Isotope	Half life	Release (kg)
Kr-85	10.7 y	1.124	Mo-99	2.8 d	7.583E-5
Sb-125	2.8 y	6.591E-4	Rh-105	35.5 h	5.85E-8
Sb-127	3.8 d	1.560E-5	Ba-140	12.8 d	1.676E-4
I-131	8.0 d	1.736E-2	Sr-90	28.6 d	6.551E-4
Te-132	3.2 d	1.151E-4	Sr-91	9.5 h	2.444E-8
I-132	2.3 h	3.247E-5	Y-92	3.7 h	2.857E-27
Xe-133	5.2 d	0.251	Ru-103	39 d	9.655E-5
I-133	20.8 h	1.689E-3	Ru-105	4.4 h	4.579E-9
I-134	0.9 h	5.756E-14	Ru-106	1.0 y	4.460E-4
Cs-134	2.1 y	0.0142	La-140	1.7 d	9.342E-6
I-135	6.6 h	6.934E-5	Ce-141	32 d	1.419E-4
Xe-135	9.1 h	2.635E-3	Ce-143	1.4 d	3.188E-6
Cs-137	30.1 y	0.147	Ce-144	284 d	1.071E-3

as I-134, Y-92 and Ru-105. Decay of the isotopes dominates the accumulation of the fission products and amount decreases. For this reason, the source term definition of the JRODOS was made time dependent and each 30 min period of savings were defined separately in order to cover all releases.

The Java based Real-Time Online Decision Support (JRODOS) code (Ievdin,et al., 2010) is used to assist emergency response teams in investigating accident transients to assess radiological impacts and decide appropriate steps to protect and ensure public safety. The code considers weather data for the selected period, geographic information about the area, and the distribution and type of public household, vegetation, and possible digestion pathways and countermeasures when analyzing the release of fission products. In this way, it is possible to provide a detailed analysis of the radiological impact, taking into account the long- and short-term effects of the dispersion.

However, since each day of the year and season brings different weather conditions and the onset of the accident can be on any day of the year and at any time of the day, the statistical approach in the previous study (Murat,et al., 2023) was used to understand the possible consequences by considering a wide range of time scales in the calendar.

The JRODOS analysis was conducted at the Peach Bottom Unit-2 site by constructing a mesh grid within a 400 km radius of the site. The constructed elevation grid and population distribution over the region under consideration are shown in Figs. 4–7. The location of the power plant and the constructed grid were kept the same as in the previous study. As can be seen from the elevation of the region, the hills and mountains are parallel to the Atlantic coast from southwest to northeast. The settlements and population density are located in the coastal region. For this reason, it is reasonable to assume that the hills may play a role in blocking winds from the coast to the interior of the continent. It is expected that the winds occur mainly in the same plain of the settlements. The selection of the region of interest was maintained as in the previous study. New York City, Philadelphia, Baltimore, and Washington DC are the most populous cities in the grid considered.

The time frame was chosen between January 1, 2019 and January 1, 2022 to take a statistical approach. The reason for considering a longer time period than in previous publication is that the average weather pattern across the mesh can be better estimated with the taking into account of more stored meteorological data. All isotopes released to the environment in the ASTEC simulation formed the source term data for the JRODOS simulation. After that, selected period of a 24-hours simulation is run with a random start time on the day using this source term. The reason for the one-day duration of the statistical analysis is that only making assessment of the risks over the selected cities not the long-term effects of the radiological consequences of the accident. More detailed analysis that includes the food chain and specific age groups considering longer time span can be done. However, in order to perform a detailed radiological release analysis, the first step should be to understand the risk factors of the population surrounding the power plant. Not only the nearest cities, but also other places in the region that were not considered due to long distances may pose a significant risk, and this is crucial for emergency response teams and decision makers to determine the necessary actions. In addition, the release in the ASTEC simulation lasted a total of 20.68 h, which means that one day is enough to simulate the entire release from the power plant.

All recorded total effective gamma dose rates among the interested meshes are shown in Fig. 4–8. The highest dose rate of 67.89 mSv/h was recorded at mesh 2594, corresponding to Baltimore, when the simulation began at 20:41 on December 13, 2019. Distribution of the dose rate over the considered domain after 6,12,18 and 24 h after release start given in Fig. 4–9. The highest recorded dose rate is well above the dose limits established by the United States Nuclear Regulatory Commission

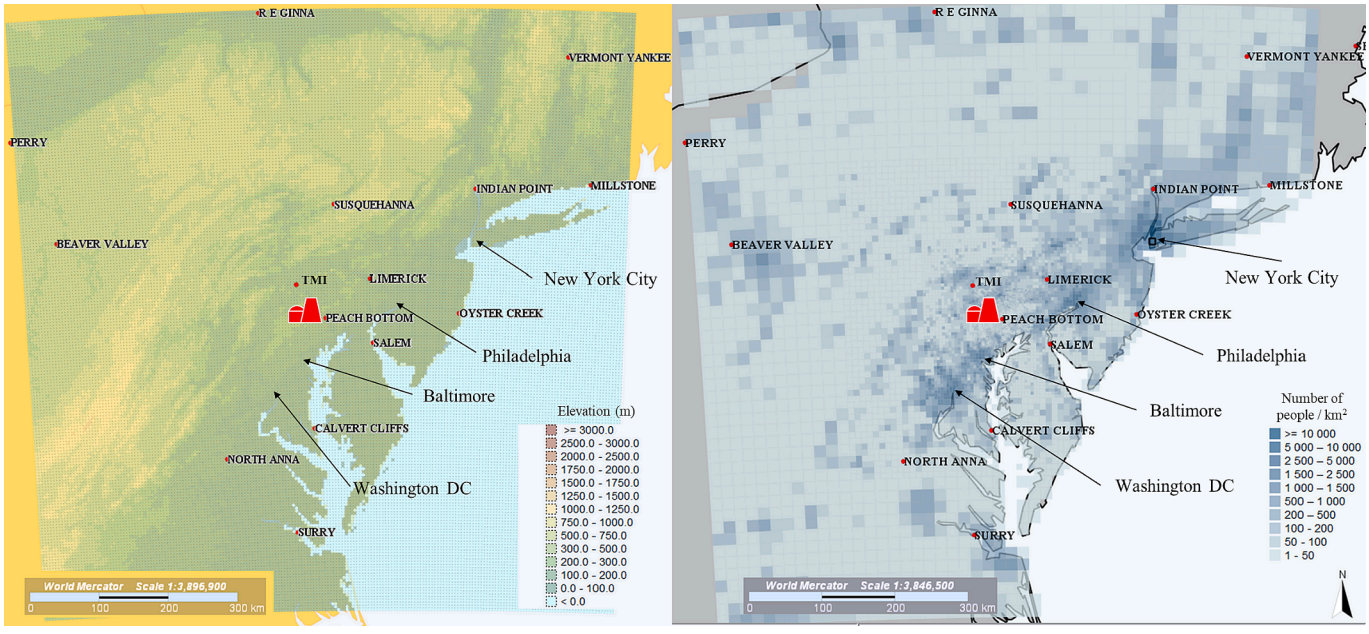

Fig. 4–7. The Peach Bottom NPP site 400 km mesh grid with elevation of the region (left) and population distribution over grid (right).

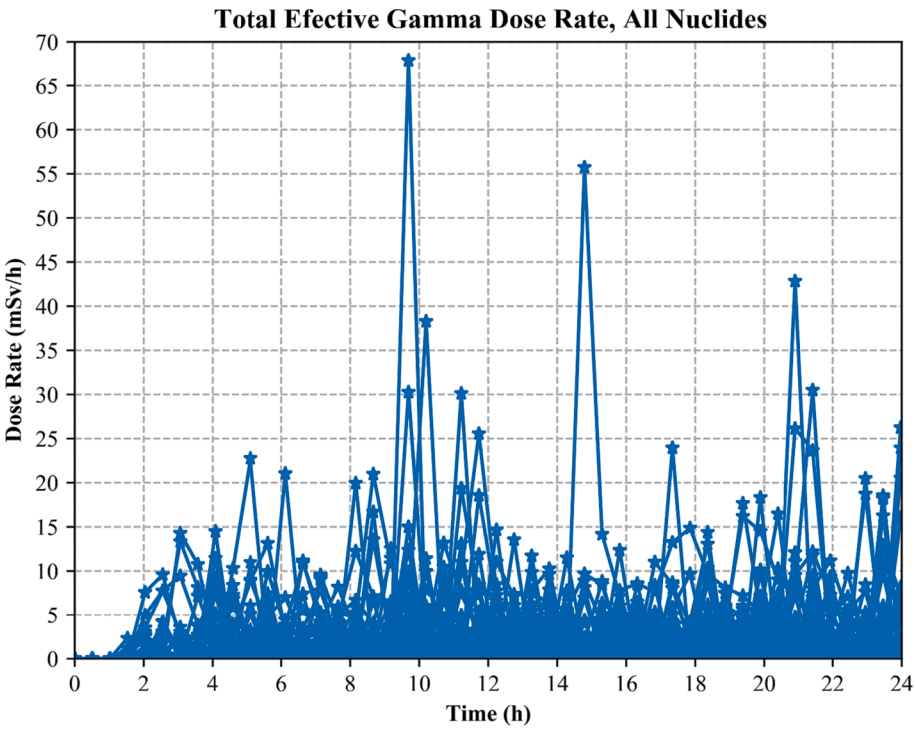

Fig. 4–8. Total effective gamma dose rates of one day simulations for three years (2019, 2020, 2021) among the interested meshes for ST-SBO transient.

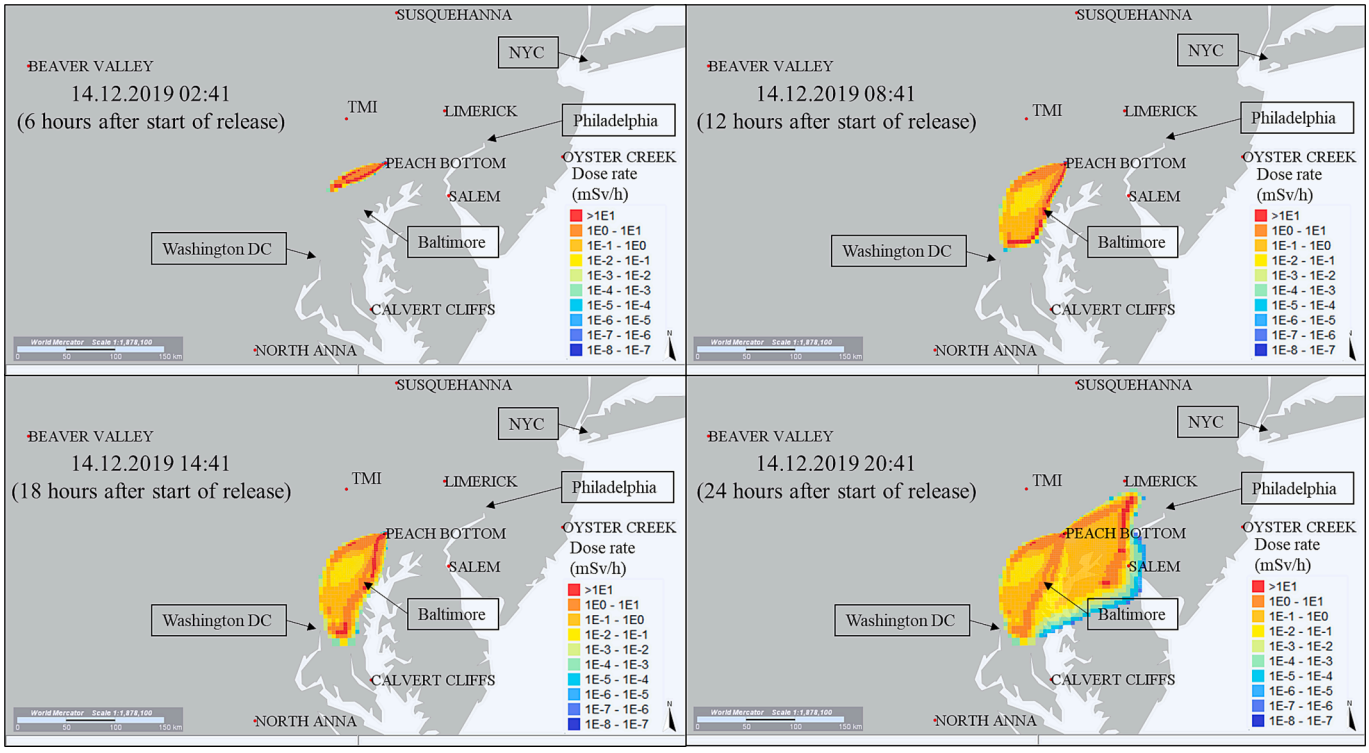

Fig. 4–9. Total effective gamma dose rate map resulted by ST-SBO scenario over the Peach Bottom Unit-2 Plant domain after 6, 12, 18 and 24 h after release start instant on 13th of December 2019 at 20:41.

(USNRC) (U.S. Nuclear Regulatory Commission, Radiation Dose Limits for Individual Members of the Public (Subpart D), 10C.F.R. § 20.1301 1991), namely 5 mSv/year for radiation workers and 1 mSv/year for the public. A statistical analysis in the previous publication with 7x7 assemblies, using a lower burnup and fission product inventory, also showed the highest dose rate at Baltimore, but at a value of 7.2 mSv/hr. An improved core and higher burnup resulted in an increase in the highest recorded total effective gamma dose rate by a factor of almost 10. Not only on the highest recorded day, but other trends in Fig. 4–8 show higher dose rates for other cases.

Number of days dose recorded for the cities for the three years analysis are 187 times for Baltimore, 45 times for Washington DC, 316

times for Philadelphia, and 529 times for New York City. Dose rate was measured 1077 times in three years (1095 days) in the grid cities considered. As expected from the elevation map wind regime covers the considered cities most of the year. Although the highest dose rate was measured in Baltimore, fission product transport and dose rate were recorded only 187 times, which is not the highest frequency among the cities considered. The most distant New York City has the highest storage frequency, which provides information about the annual wind regime. Not only the amount of dose rate, but also the frequency of mesh savings gives the risk factor in the region. Since the risk is considered as the multiplication of magnitude and frequency, the annual regime and statistical analysis help to understand the risk factor around the power plant.

5. Analysis of the ST-SBO SOSRV for Peach Bottom Unit-2

Activated modules and steady state analysis results are identical with ST-SBO analysis done in previous chapter since the only transient scenario was changed. Version of the code also did not changed.

5.1. Short term Station Black-Out with Stuck Open Safety Relief Valve Accident

The increase in power and the change in the design of the fuel assembly with higher burnup lead to a new configuration, so the approach to severe accident analysis must also be updated. In the accident analysis study for Peach Bottom Unit-2 NPP (Bixler et al., 2013), new fuel assemblies and the accident ST-SBO were considered as one of the main factors for the frequency of core damage. In addition to the selection of transients, based on expert judgment, safety system responses in the station blackout scenario were also considered. One of the responses considered in ST-SBO, failure of a safety relief valve. Based on the manufacturer's data for the operation of the valve and the failure logs, the operation of a safety relief valve will cease after 270 consecutive cycles. In the ASTEC modeling, the SRV-1 safety relief valve (Leonard, Gauntt and Powers, 2007) with the lowest pressure set point was selected for operation and considered open after 270 open/close cycles.

5.1.1. Main results of ST-SBO SOSRV transient

The sequence of events, including all considered ST-SBO results, can be found in Table 5–1. Manual operation of a safety relief valve until the vessel is depressurized is not considered in ST-SBO SOSRV transient. The section for the stuck open SRV-1 was added to the table and progression of the accident and key events given chronological order.

SRV-1 operation between pressure set points was shown in Fig. 5–1 with previous ST-SBO analysis results. The dashed blue line represents the old fuel assembly type for ST-SBO transient, the red solid line represents the new fuel assembly type for ST-SBO transient, and the green dash-dotted line represents the new fuel assembly type for the ST-SBO SOSRV scenario. The following figures (Fig. 5–2, Fig. 5–3, Fig. 5–5) show the same trend in color and line type for the considered cases. The pressure cycles in ST-SBO SOSRV transient show a higher operating level because the manual operation of a safety valve was set to lower pressure set points. After 270 consecutive cycles, SRV-1 remains open and the pressure starts to decrease rapidly at 5835 s. The opening of the safety relief valve plays a role in depressurizing the core. However, this role is not related to the water level in the core as was the case with the previous transients.

The water levels in the vessel during the three transients considered so far are shown in Fig. 5–2. At the beginning, thanks to the updated recirculation line, a gradual decrease is also observed in the case ST-SBO SOSRV. The previously considered ST-SBO scenario with updated core and recirculation line also follows a safety valve operation until the ADS actuation. The level of water follows a similar decrease with the new ST-SBO SOSRV calculation. Since the 5 safety valves of the ADS system are not opened, a sudden rise in water level due to pressure drop and steam flashes was not observed with the new transient. The release of steam and fission products was ensured only by one safety valve and the total release lasted longer and was stored at 13,489 s.

Table 5-1
Comparison of the sequence of events between new and old design fuel assemblies in Peach Bottom Unit-2 ASTEC Model for ST-SBO and ST-SBO SOSRV scenarios.

Sequence of Events	Time (s) (10x10) ST-SBO SOSRV	Time (s) (10x10) ST-SBO	Time (s) (7x7) ST-SBO (Murat,et al., 2023)
SRV-1 starts operation	0	0	0
SRV-1 stops operation, Manual operation of a SRV starts	–	200	200
First cladding creep rupture, start of the fission product release	530	524	1037
First material slump in lower plenum	633	622	1142
First slump of corium with fission products in lower plenum	651	643	1158
First appearance of a cavity in core	662	648	1167
Manual operation of a SRV stops, ADS actuates	–	4782	3867
Stuck open SRV-1	5835	–	–
First total core uncovery	13,489	9959	6772
Lower head vessel failure	22,777	21,616	13,361
PCV head flange failure	26,701	26,137	13,415
Basemat rupture	116,575	100,576	88,142

The prolonged presence of water and steam in the core sustained the oxidation reaction. Compared to previous transients with new fuel assemblies, the operation of a safety valve and the assumption that it would remain open delayed the total core uncovery by about an hour. At the end of the accident in the reactor vessel, the total hydrogen production for ST-SBO SOSRV was 2447.0 kg. Compared to previous results, which were 2138.3 kg for 10x10 fuel assemblies and 1847.6 kg for 7x7 fuel assemblies for ST-SBO transient, the larger hydrogen production is due to the fact that the metallic structure in the core was exposed to the steam environment for a longer period of time. Since the coolability of the core can only be measured when water enters the core, the disadvantage of the water and steam environment can lead to stronger chemical reactions and greater heat release. For this reason, depressurization of the vessel and water injection amount, if an emergency cooling system was present, determine the progression of the severe accident.

The failure of the lower head was recorded at 22,777 s for ST-SBO SOSRV and the failure mesh at the lower plenum wall is between 1.85 m and 2.13 m axially from the bottom of the vessel. As expected due to the higher axial height of the failure point at the lower plenum wall, the ejected corium mass is lower compared to the other ST-SBO transient scenarios considered and is recorded to be 67.26 tons (see Fig. 5–4). The accumulation of molten material is not as high as in the previous ST-SBO scenario with new fuel assemblies, which is why the ejected corium is almost one third of its mass. The water and steam environment has helped to cool the core at the lower elevations and reduce the accumulation of corium in the lower plenum.

The comparison of the failure times of the lower head is determined by the cooling ability in the vessel and lower head and shows the failure time based on the water intake in the lower head. However, the failure points and the corresponding ejected corium masses are so different that they do not fit into a certain connection in between. The scenario examined in a previous study (Murat,et al., 2023) ST-SBO with 7x7 fuel assemblies resulted in an ejection of about 152 tons of corium, and the same scenario with updated 10x10 modern fuel assemblies showed that about 210 tons of magma ejected from the lower plenum. It could be that

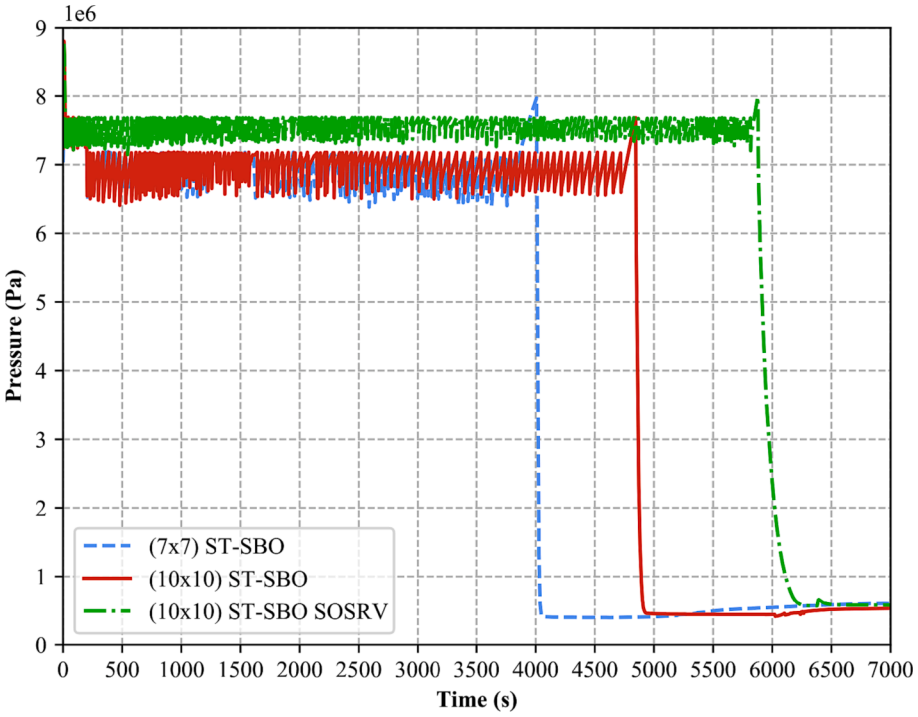

Fig. 5–1. Comparison of the vessel pressure between new and old design fuel assemblies during depressurization operation of the vessel.

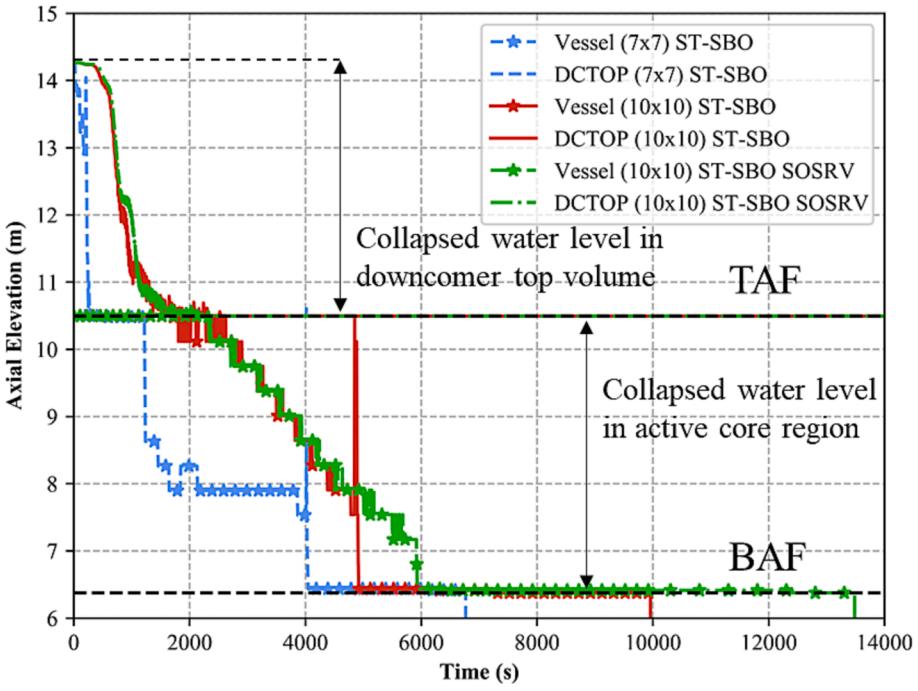

Fig. 5–2. Comparison of water level between new and old design fuel assemblies inside the vessel and top of the downcomer for ST-SBO and ST-SBO SOSRV scenarios.

a higher mass and energy level was the result from the beginning, but ST-SBO SOSRV with new 10x10 fuel assemblies showed 67 tons ejection, which is significantly less than other transients. In addition, the Peach Bottom Unit-2 MELCOR model with the ST-SBO transient (Carbajo, 1993) with older 7x7 fuel assemblies predicted 180 tons of corium release from the lower plenum with the stand-alone MELCOR code. Implementing the lower plenum penetration failure model and using the MELCOR/CORBH version of the code in the same study resulted in 280 tons of corium release. The failure point for the MELCOR/CORBH case was first predicted for the small penetration points and then a larger breach was calculated at the lower head wall.

The severe accident study of the Peach Bottom Plant with MELCOR (Bixler et al., 2013), where stochastic failure of the safety valve was expected after a certain operating cycle, also had results related to failure of the lower head vessel. Penetration failure, one of the mechanisms for lower head loss of integrity, was not explicitly modeled in the

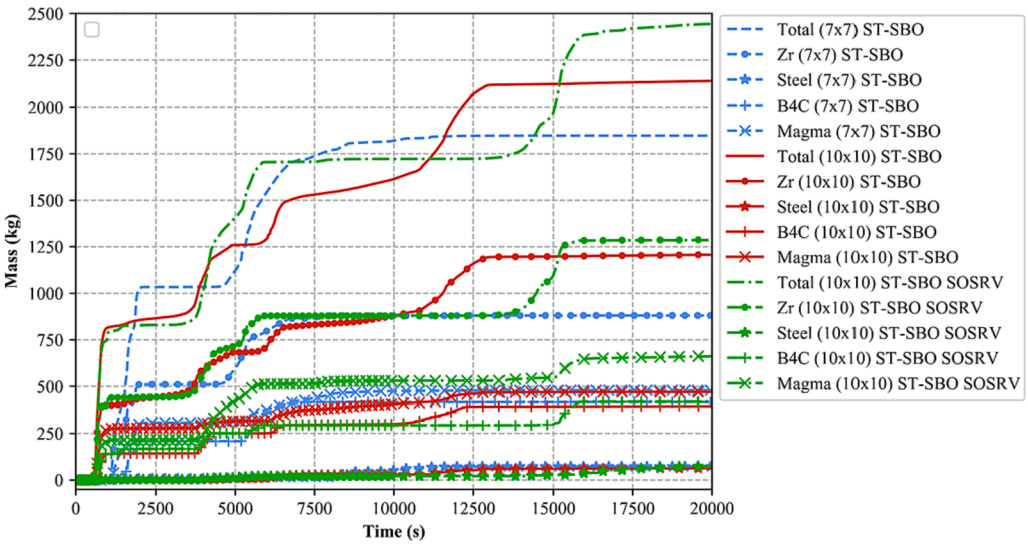

Fig. 5–3. Comparison of generated hydrogen mass between new and old design fuel assemblies caused by the oxidation of the structures for ST-SBO and ST-SBO SOSRV scenarios.

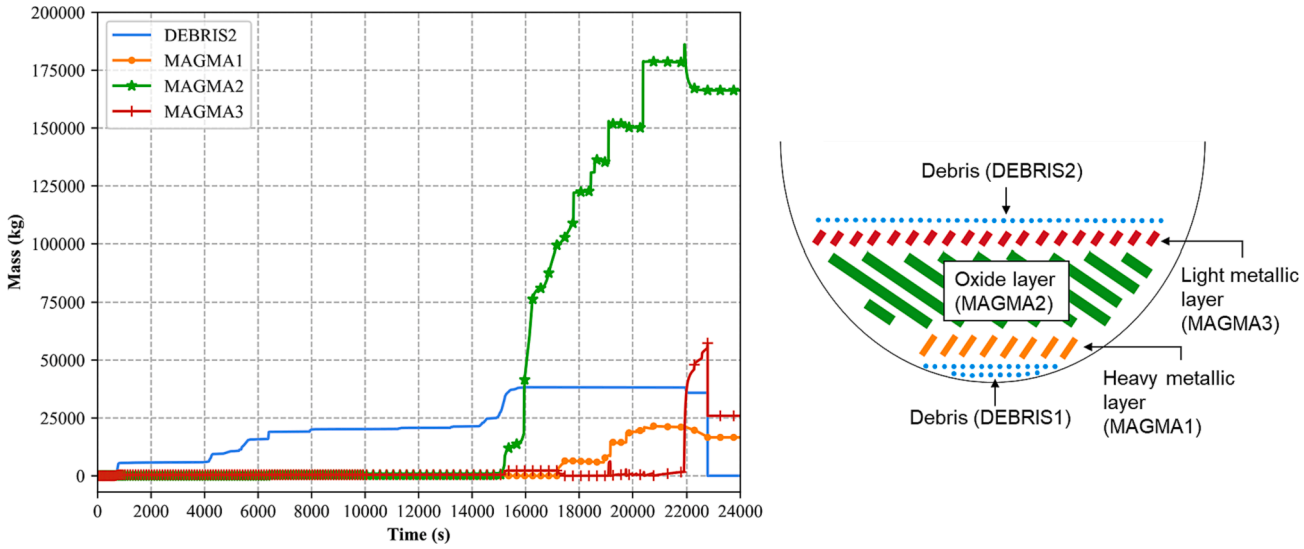

Fig. 5–4. Corium mass accumulation for 10x10 fuel assembly ST-SBO SOSRV scenario up to failure in the lower plenum (left) and ASTEC typical debris configuration in the lower plenum (right).

MELCOR model because the integrity model was not present, which also plays a role in the uncertainties of the model. Although the lower head of the BWR has greater volume and water absorption capacity, as well as structural materials that can be used to store excess heat, the number of penetrations and the durability of the connection points have great potential, as shown for the different scenarios and codes considered, which predict very different amounts of corium ejection. Timing of the lower head failure and failure mechanism have significant effect for accident progression analysis, fission product release, identification of ex-vessel phenomena, and the containment failure.

Estimation of the failure at the weldings of the penetration points on the lower head caused by the molten material was made and highlighted in the previous special study devoted lower head failure analysis for the light water reactors (Rempe,Chavez and Thinnes, 1993). Models have been proposed to simulate possible failure points and mechanism for the penetration points but they need to be supported by the experimental programs.

The joint work was developed for PWR lower head analysis and creep failure study. The results of the OECD Lower Head Failure (OLHF) program (Humphries et al., 2002) can be highlighted here. The program was developed to provide data for the failure time and sizes of the PWR lower head model under pressure and thermal loading. A scaled- down model of the lower head was used and a series of experiments were performed. Test number 4 (OLHF-4) considered the PWR instrumentation tube on the lower head and was compared with the OLHF-2 test performed at the same pressure without penetration points. In the case of OLHF-4, where integrity was lost earlier, a small fracture was observed at the weld of the instrument tube.

Only the operation of the one safety valve extended time spent in-vessel and resulted in a delay in total core uncover and vessel failure. However, the primary containment failure showed very similar results for the ST-SBO and ST-SBO SOSRV transients with new fuel assemblies (see Fig. 5–5). In both cases, the second failure mode was activated, corresponding to the failure of the drywell head and the activation of the connection between the drywell zone and the refueling zone. Since the operation of the safety valves and ADS for the case ST-SBO pressure and temperature in the drywell zone were built up almost at the same rate, and after the failure of the bottom head the pressure and temperature

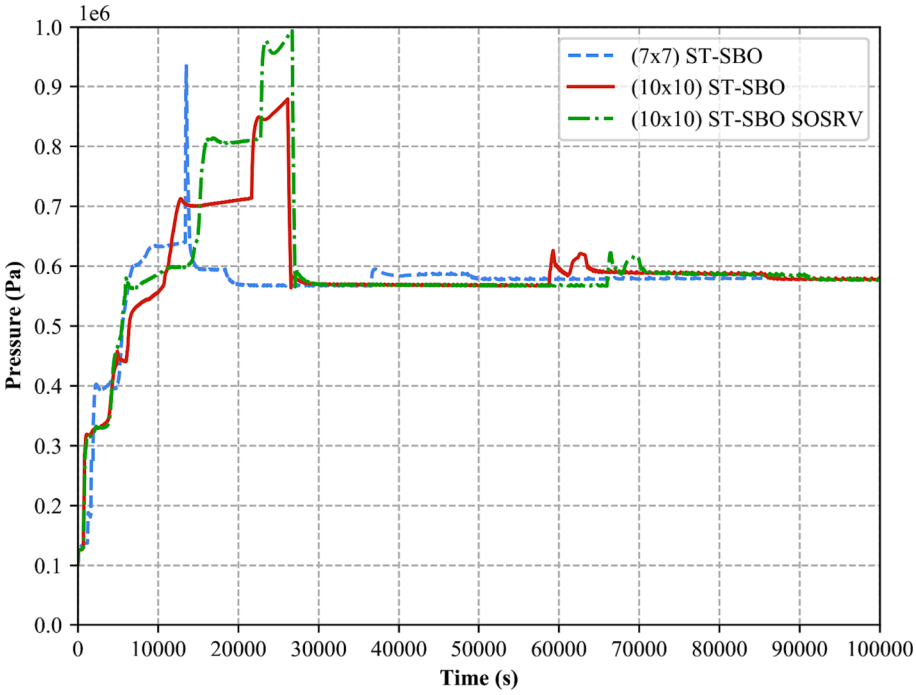

Fig. 5–5. Comparison of the Drywell Zone pressure between new and old design fuel assemblies for ST-SBO and ST-SBO SOSRV scenarios.

Table 5-2
Fission products mass inventory and their retention fractions in the considered domains for ST-SBO SOSRV transient.

Elements	Inventory (kg)	Primary	Containment	Environment
Kr	68.60	0.011	0.491	0.356
Xe	1025.79	0.011	0.491	0.356
I	36.66	0.040	0.791	0.020
Sb	2.81	0.033	0.695	0.001
Te	93.41	0.166	0.492	8.53E-4
Ag	7.30	0.182	0.670	0.001
Cs	556.56	0.095	0.772	0.001
Rh	79.54	3.27E-5	3.91E-4	2.83E-7
Mo	644.51	0.134	0.424	4.31E-4
Ba	290.09	0.081	0.322	7.75E-4
Sr	166.72	0.060	0.013	2.8E-5
Y	87.65	4.14E-5	9.77E-6	6.95E-8
Nb	3.80	0.0	0.0	0.0
Ru	479.17	0.024	0.271	2.61E-4
Ce	502.68	0.027	0.096	2.25E-4
La	236.88	0.005	0.017	3.49E-5
Eu	27.98	0.002	0.006	1.26E-5

reached the considered limits in a short time, a similar failure of the PCV head flange was observed.

Fission product inventory which outcomes of the CASMO5 analysis and concluded element fractions in considered domains, which are CESAR volumes for primary, CPA zones for the containment and environment, are given in Table 5–2. Since the transient case for the ST-SBO SOSRV took longer period up to basemat failure than ST-SBO, release to the environment zone is higher. Environmental release of the ST-SBO SOSRV transient used as source term for the following dispersion analysis with JRODOS.

5.2. Statistical Analysis of the Fission Products Dispersion and Radiological Impact of ST-SBO SOSRV Scenario with JRODOS

Total radioactive fission products released to the environment at the end of ST-SBO SOSRV transient with ASTEC simulation recorded an activity of 2.712E+18 Bq. Selected main radioactive fission products

Table 5-3
Total mass of radioactive fission products released to the environment at the end of ST-SBO SOSRV scenario.

Isotope	Half life	Release (kg)	Isotope	Half life	Release (kg)
Kr-85	10.7 y	1.513	Mo-99	2.8 d	1.121E-4
Sb-125	2.8 y	1.435E-3	Rh-105	35.5 h	8.181E-7
Sb-127	3.8 d	3.292E-5	Ba-140	12.8 d	1.594E-3
I-131	8.0 d	1.349E-2	Sr-90	28.6 d	2.789E-3
Te-132	3.2 d	2.803E-4	Sr-91	9.5 h	7.554E-8
I-132	2.3 h	2.183E-5	Y-92	3.7 h	1.207E-29
Xe-133	5.2 d	0.330	Ru-103	39 d	1.267E-3
I-133	20.8 h	1.151E-3	Ru-105	4.4 h	3.015E-8
I-134	0.9 h	1.397E-15	Ru-106	1.0 y	5.872E-3
Cs-134	2.1 y	3.327E-2	La-140	1.7 d	9.025E-5
I-135	6.6 h	3.428E-5	Ce-141	32 d	1.173E-3
Xe-135	9.1 h	2.614E-3	Ce-143	1.4 d	2.413E-5
Cs-137	30.1 y	0.345	Ce-144	284 d	8.889E-3

masses are presented in Table 5–3.

The same mesh grid and locations for the statistical analysis of fission product dispersion of the ST-SBO transient scenario were also used for the ST-SBO SOSRV, for the same cities and the corresponding meshes. The total one-day release and recorded isotopes were used as the source term, and a 24-hour simulation schedule was run for the 3 years (2019, 2020, 2021) for the statistical analysis.

The result of the statistical analysis is shown in Fig. 5–6 The highest recorded total effective gamma dose rate of 119.46 mSv/h was found in Baltimore (mesh 2594). For the highest dose rate scenario, the release start date was 22:55 on October 28, 2020. Distribution of the dose rate over the considered domain after 6,12,18 and 24 h after release start given in Fig. 5–7. Compared to previous ST-SBO transients involving both new and old type fuel assemblies, the highest total effective gamma dose rate was detected in the transient of the safety valve considered open. Not only the highest value, but also the general trend in Fig. 5–6 shows that the recorded dose rate is higher in all considered cities.

The number of city savings for the three-year statistical analysis are 199 times for Baltimore, 39 times for Washington DC, 307 times for Philadelphia, and 528 times for New York City. Although the start date for the release was randomized in each daily simulation, the daily and

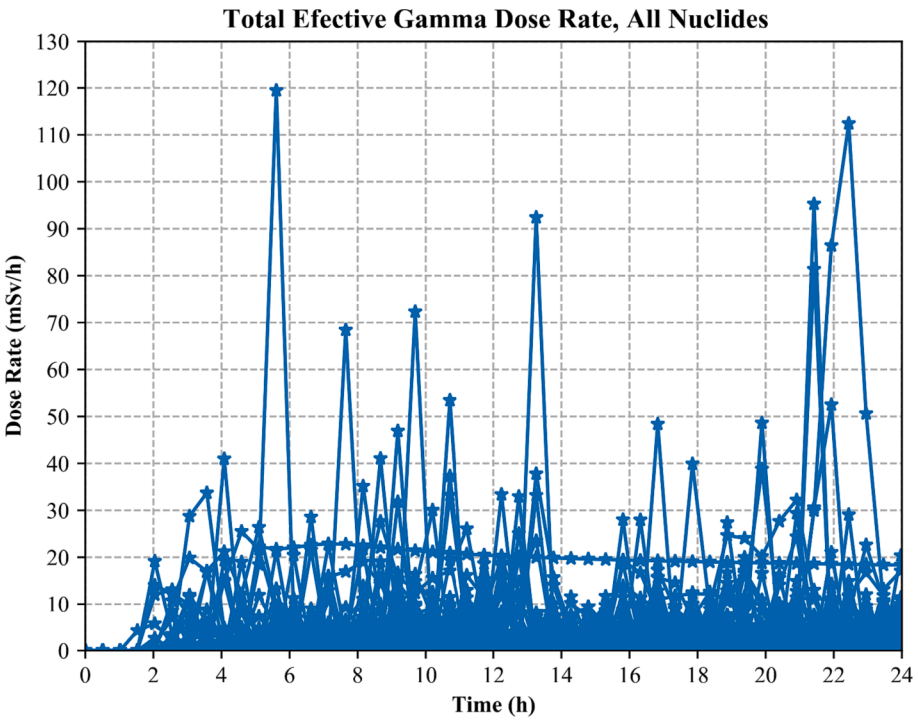

Fig. 5–6. Total effective gamma dose rates of one day simulations for three years (2019, 2020, 2021) among the interested meshes for ST-SBO SOSRV transient.

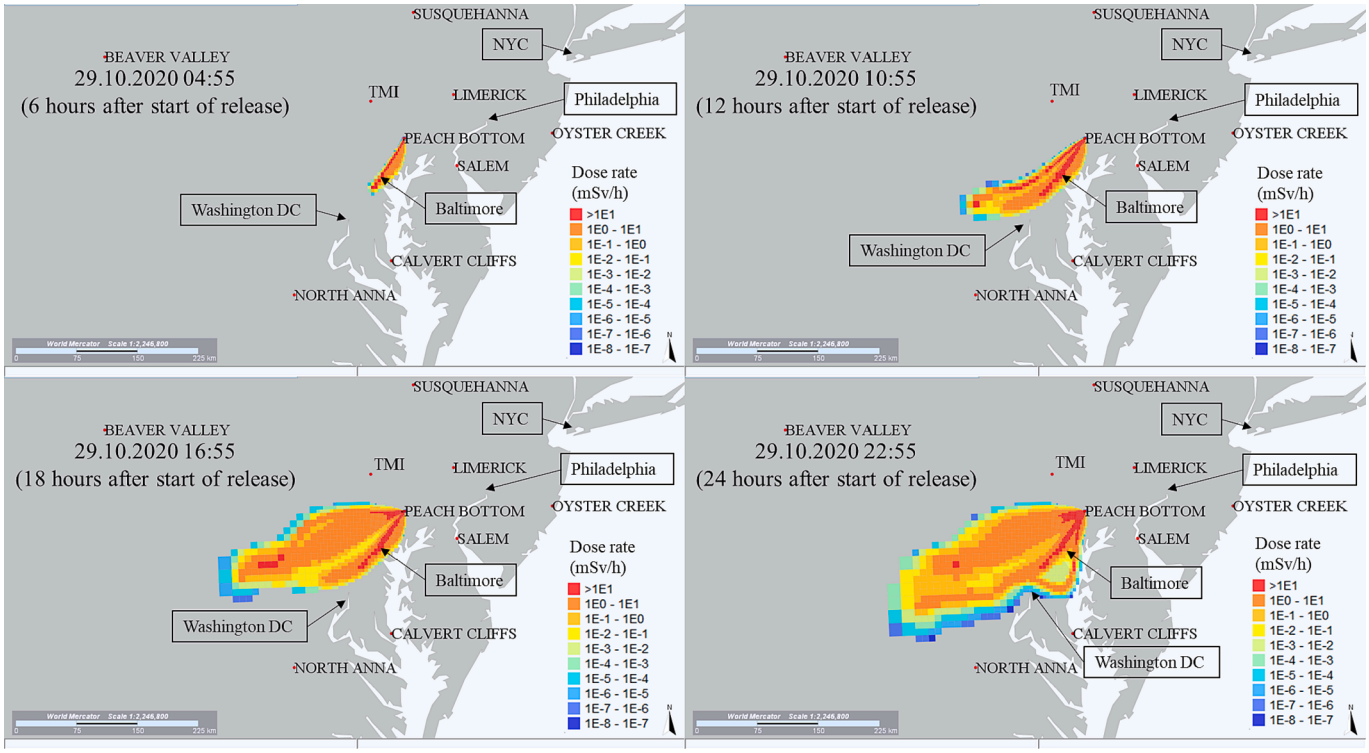

Fig. 5–7. Total effective gamma dose rate map resulted by ST-SBO SOSRV scenario over the Peach Bottom Unit-2 Plant domain after 6, 12, 18 and 24 h after release start instant on 28th of October 2020 at 22:55.

annual weather patterns still show the same behavior for the frequency of savings. The highest recorded dose rates expected for cities near the power plant do not necessarily mean that these meshes always receive the radiation plume due to carrier winds.

6. Conclusion and Outlook

By updating the Peach Bottom Unit-2 ASTEC model and using the CASMO5 code to account for new fuel assembly types and higher burnup values, the selected transient from the previous study and new transient were applied. After that, fission products transported to the environment

played the role of source term for the JRODOS analysis, and the time period was increased to 3 years based on the recommendation of the JRODOS team at KIT to account for average weather conditions. The combination of these three codes allows the user to simulate the severe accident of the initiating event, taking into account the fission product inventory and the radiological impact of the transient in terms of public safety.

The burnup of the modern fuel assemblies in the BWR core increases up to 45–50 MWd/t and results in a significant amount of fission products that pose potential risks to public safety and the environment. To compare the magnitude of the difference between 10x10 and 7x7 fuel assembly types and the burnup values considered, the same transient ST-SBO was used. The model improvement was not only for the fuel assembly, but also for the recirculation line, which provided a better representation of the flow rate and connections. Although the water level and accident history were estimated with a higher amount of water in the core, the decay heat and exothermic chemical interactions dominated in terms of excess heat in the core and led to the failure of the vessel and containment with a higher amount of fission products compared to previous work that only addressed 7x7 fuel assemblies with lower burnup.

The considered ST-SBO SOSRV scenario, involving only the operation of a safety valve and its stochastic failure, was performed for the Peach Bottom Plant. The sensitivity analysis in the previous study (Bixler et al., 2013) showed that the different number of times the safety valve was operated had minor differences in the source term released to the environment and the timing of the bottom head failure. However, when the emergency Reactor Core Isolation Coolant System (RCIC) was operated for a certain time at the beginning, the number of actuations of the safety valve shows significant differences thereafter. Since the analysis was selected for the worst-case scenario and fast running cases, the importance of the systems and their sensitivity could be considered as the next step for the ASTEC simulation of the Peach Bottom Plant.

The mode of failure of the lower head in the ASTEC model considers only the loss of integrity of the lower head wall. Since the MELCOR studies and ASTEC analysis show that the extent of corium ejection is scattered, and the experimental analysis shows that the timing and extent of failure are in a very scattered spectrum, the implementation of a detailed model and failure mode for the lower head of the BWR greatly increases the understanding of severe accident progression and the accuracy of environmental release prediction.

The total effective gamma dose rate and the statistical analysis of the considered geographical meshes, corresponding to the most populated cities, were carried out for three years to take into account a larger time span and the average meteorological regime. In the case of ST-SBO and ST-SBO SOSRV, the storage frequencies showed a similar trend over the mesh. The highest recorded dose and the received doses are higher on average for the ST-SBO SOSRV scenario, however, the vessel failure was recorded about 1000 s later. The longer the accident progresses in the vessel, the more fission products can be transferred from the vessel to the containment. After the failure of the lower head vessel, the in-vessel accident progression and the calculation in the associated modules stops. However, since the selection of the release time in JRODOS is random each day, the same day may show different results and pathways. To drive this statistical analysis, the number of analyzes for the considered meshes can be increased and one can create a pool of samples of different release times for each day. Increasing the number of samples for each day creates a distribution that provides information about the dose reception probability of the considered meshes. This information can be used to create a risk map for the future study. The probability of receiving a given dose in the event of a radiological release can be used to complete a severe accident analysis and help decision makers determine countermeasures.

CRediT authorship contribution statement

Onur Murat: Writing – review & editing, Writing – original draft, Visualization, Software, Methodology. **Victor Sanchez-Espinoza:** . **Fabrizio Gabrielli:** Supervision. **Shisheng Wang:** Supervision. **Robert Stieglitz:** Supervision. **Cesar Queral:** Supervision.

Declaration of competing interest

The authors declare that they have no known competing financial interests or personal relationships that could have appeared to influence the work reported in this paper.

Data availability

The data that has been used is confidential.

Acknowledgement

The corresponding author is funded by Republic of Turkey Ministry of National Education during his Ph.D. studies.

References

Bixler, N., Gauntt, R., Joseph, L., Jones, M., 2013. State-of-the-Art Reactor Consequence Analyses Project. U.S.NRC, Albuquerque, New Mexico.

Carbajo, J.J. 1993. *Severe Accident Source Term Characteristics for Selected Peach Bottom Sequences Predicted by the MELCOR Code, NUREG/CR-5942.* Oak Ridge, TN 37831-6285: U.S. Nuclear Regulatory Commission.

Chatelard, P., Belon, S., Bosland, L., Carénini, L., Coindreau, O., Cousin, F., Marchetto, C., Nowack, H., Piar, L., Chailan, L., 2016. Main modelling features of the ASTEC V2.1 major version. Ann. Nucl. Energy 93, 83–93. https://doi.org/10.1016/j.anucene.2015.12.026.

Chatelard, P., F. Gabrielli, F. Fichot, H. Bonneville, C. Bouillet, S. Belon, L. Chailan, and V.H. Sanchez Espinoza. 2017. *Contribution of ASTEC numerical simulations to the understanding of the Fukushima accidents.* Vienna: IAEA Workshop on Advances in Understanding the Progression of Severe Accidents in Boiling Water Reactors.

EPRI, 2010. MAAP4 Applications Guidance, Desktop Reference for Using MAAP4 Software, Revision 2. Electric Power Research Institute, Palo Alto, CA.

Exelon Generation Company. 2018. "Subsequent Licence Renewal Application, Peach Bottom Atomic Power Station Units 2 and 3." Accessed 05 26, 2023. https://www.nrc.gov/docs/ML1819/ML18193A773.pdf.

Gauld, I., Mertyurek, U., 2018. Margins for the Uncertainty in the Predicted Spent Fuel Isotopic Inventories for BWR Burnup Credit, NUREG/CR-7251. U.S. Nuclear Regulatory Commission, Oak Ridge, TN.

Hu, Jianwei, Ian C. Gauld, Joshua L. Peterson, and Stephen M. Bowman. 2016. *US Commercial Spent Nuclear Fuel Assembly Characteristics: 1968-2013, NUREG/CR-7227.* Oak Ridge, TN 37831-6170: U.S. Nuclear Regulatory Commission.

Humphries, L.L., T.Y. Chu, J. Bentz, R. Simpson, C. Hanks, W. Lu, B. Antoun, C. Robino, J. Puskar, and P. Mongabure. 2002. "OECD Lower Head Failure Project Final Report." Accessed July 5, 2023. https://www.oecd-nea.org/jcms/pl_25806/sandia-lower-head-failure-project.

Humphries, L.L., B.A. Beeny, F. Gelbard, D.L. Louie, and J. Phillips. 2017. *MELCOR Computer Code Manuals, Vol. 1: Primer and Users' Guide, Verson 2.2.9541.* Albuquerque: Sandia National Laboratories.

Ievdin, I., Trybushnyi, D., Zheleznyak, M., Raskob, W., 2010. RODOS re-engineering: aims and implementation details. Radioprotection 45, 181–189. https://doi.org/10.1051/radiopro/2010024.

Kolaczkowski, A.M., Cramond, W.R., Sype, T.T., Maloney, K.J., Wheeler, T.A., Daniel, S. L., 1989. Analysis of Core Damage Frequency: Peach Bottom, Unit 2 Internal Events, NUREG/CR-4550, Vol. 4. Sandia National Laboratories, Albuquerque.

Larsen, N.H., 1978. Core Design and Operating Data for Cycles 1 and 2 of Peach Bottom 2, NP-563. General Electric Company, California.

Lawing, C., Palmtag, S., Kropaczek, D., 2021. Oak Ridge National Laboratory Analysis of Approximations in Modeling of BWR Bundle Void Distributions, ORNL/SPR-2021/2241. Oak Ridge National Laboratory, Oak Ridge, TN.

Leonard, M.T., Gauntt, R.O., Powers, D.A., 2007. Accident Source Terms for Boiling Water Reactors with High Burnup Cores Calculated Using MELCOR 1.8.5. Sandia National Laboratories, Albuquerque.

Leonid, A., Bolshov, S.D., Kirill, E.K., Arkady, Strizhov Valery, F., 2019. Results of SOCRAT code development, validation and applications for NPP safety assessment under severe accidents. Nucl. Eng. Design 341, 326–345. https://doi.org/10.1016/j.nucengdes.2018.11.013.

Marshall, W., Ade, B.J., Stephen, M.-G., Bowman, J.S., 2016. Axial Moderator Density Distributions, Control Blade Usage, and Axial Burnup Distributions for Extended BWR Burnup Credit, NUREG/CR-7224. U.S. Nuclear Regulatory Commission, Oak Ridge, TN.

Martinez, J.S., Ade, B.J., Bowman, S.M., Gauld, I.C., Ilas, G., Marshall, W.J., 2015. In: Impact of Modelling Choices on Inventory and in-Cask Criticality Calculations for Forsmark 3 BWR Spent Fuel. ICNC, Charlotte, North Carolina, pp. 361–374.

Murat, O., Sanchez-Espinoza, V., Gabrielli, F., Stieglitz, R., Queral, C., 2023. Analysis of Short Term-Station Blackout accident at the Peach Bottom Unit-2 reactor with ASTEC including the estimation of the radiological impact with JRODOS. Nucl. Eng. Design 406. https://doi.org/10.1016/j.nucengdes.2023.112227.

Narabayashi, T., Yamazaki, Y., Kobayashi, H., Shakouchi, T., 2006. Flow Analysis for Single and Multi-Nozzle Jet Pump. JSME Internat. J. Series B 49, 933–940. https://doi.org/10.1299/jsmeb.49.933.

Radaideh, M.I., Price, D.R., 2018. Criticality and uncertainty assessment of assembly misloading in BWR transportation cask. Ann. Nucl. Energy 113, 1–14. https://doi.org/10.1016/j.anucene.2017.11.006.

Radaideh, M.I., Price, D., O'Grady, D., Kozlowski, T., 2019. Advanced BWR criticality safety part I: Model development, model benchmarking, and depletion with uncertainty analysis. Prog. Nucl. Energy 113, 230–246. https://doi.org/10.1016/j.pnucene.2019.01.010.

Rempe, J.L., Chavez, S.A., Thinnes, G.L., 1993. Light Water Reactor Lower Head Failure Analysis, NUREG/CR-5642. U.S. Nuclear Regulatory Commission, Idaho.

Rhodes, Joel D., Rodolfo M. Ferrer, and Joshua M. Hykes. 2022. *CASMO5 A Fuel Assembly Burnup Program User's Manual.* Idaho Falls, Idaho: SSP-07/431 Rev. 21.

Rochman, Dimitri, Alexender Vasiliev, Hakim Ferroukhi, Ana Munoz, Miriam Vazquez Antolin, Marta Berrios Torres, Carlos Casado Sanchez, Teodosi Simeonov, and Ahmed Shama. 2022. "Analysis of ENRESA BWR samples: nuclide inventory and decay heat." *Nuclear Science and Technologies* 8 (9). 10.1051/epjn/2022007.

Sehgal, B.R., 2012. Nuclear Safety in Light Water Reactors Severe Accident Phenomenology, 1st. Academic Press. 10.1016/C2010-0-67817-5.

U.S. Nuclear Regulatory Commission, 1990. Severe Accident Risks: An Assessment for Five U.S. Nuclear Power Plants, NUREG-1150. United States Nuclear Regulatory Commission, Washington.

U.S. Nuclear Regulatory Commission. Radiation Dose Limits for Individual Members of the Public (Subpart D), 10 C.F.R. § 20.1301. https://www.ecfr.gov/current/title-10/chapter-I/part-20/subpart-D/section-20.1301 1991 Accessed 11 16, 2022.

U.S. Nuclear Regulatory Commission. 2019. "Peach Bottom Atomic Power Station, Units 2 and 3, Revision 27 to Updated Final Safety Analysis Report, Chapter 1.0." April. Accessed June 23, 2023. https://www.nrc.gov/docs/ML1911/ML19114A125.pdf.

Wielenberg, A., Lovasz, L., Pandazis, P., Papukchiev, A., Tiborcz, L., Schöffel, P.J., Spengler, C., Sonnenkalb, M., Schaffrath, A., 2019. Recent improvements in the system code package AC2 2019 for the safety analysis of nuclear reactors. Nuc. Eng. Design 354, 110211. https://doi.org/10.1016/j.nucengdes.2019.110211.